

The Mosaic Structure of Plasma Bulk Flows in the Earth's Magnetotail

1 November 1995

Prepared by

M. ASHOUR-ABDALLA and R. L. RICHARD
Institute of Geophysics and Planetary Physics
University of California
Los Angeles, California

L. M. ZELENYI
Space Research Institute
Moscow, Russia

V. PEROOMIAN
Space and Environment Technology Center
Technology Operations
The Aerospace Corporation

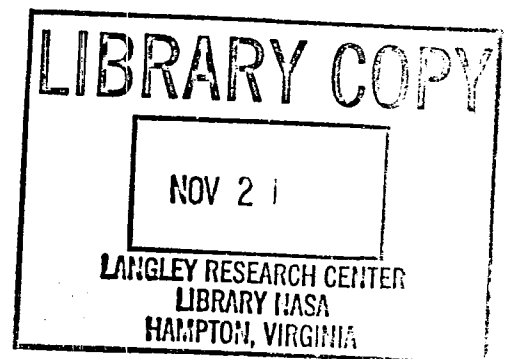
and

J. M. BOSQUED
Centre d'Etude Spatiale des Rayonnements
Toulouse, France

Prepared for

NASA
Goddard Space Flight Center
Greenbelt, Md 20771

Grant No. NAG5-1100



Engineering and Technology Group

PUBLIC RELEASE IS AUTHORIZED

TECHNOLOGY OPERATIONS

The Aerospace Corporation functions as an "architect-engineer" for national security programs, specializing in advanced military space systems. The Corporation's Technology Operations supports the effective and timely development and operation of national security systems through scientific research and the application of advanced technology. Vital to the success of the Corporation is the technical staff's wide-ranging expertise and its ability to stay abreast of new technological developments and program support issues associated with rapidly evolving space systems. Contributing capabilities are provided by these individual Technology Centers:

Electronics Technology Center: Microelectronics, VLSI reliability, failure analysis, solid-state device physics, compound semiconductors, radiation effects, infrared and CCD detector devices, Micro-Electro-Mechanical Systems (MEMS), and data storage and display technologies; lasers and electro-optics, solid state laser design, micro-optics, optical communications, and fiber optic sensors; atomic frequency standards, applied laser spectroscopy, laser chemistry, atmospheric propagation and beam control, LIDAR/LADAR remote sensing; solar cell and array testing and evaluation, battery electrochemistry, battery testing and evaluation.

Mechanics and Materials Technology Center: Evaluation and characterization of new materials: metals, alloys, ceramics, polymers and composites; development and analysis of advanced materials processing and deposition techniques; nondestructive evaluation, component failure analysis and reliability; fracture mechanics and stress corrosion; analysis and evaluation of materials at cryogenic and elevated temperatures; launch vehicle fluid mechanics, heat transfer and flight dynamics; aerothermodynamics; chemical and electric propulsion; environmental chemistry; combustion processes; spacecraft structural mechanics, space environment effects on materials, hardening and vulnerability assessment; contamination, thermal and structural control; lubrication and surface phenomena; microengineering technology and microinstrument development.

Space and Environment Technology Center: Magnetospheric, auroral and cosmic ray physics, wave-particle interactions, magnetospheric plasma waves; atmospheric and ionospheric physics, density and composition of the upper atmosphere, remote sensing using atmospheric radiation; solar physics, infrared astronomy, infrared signature analysis; effects of solar activity, magnetic storms and nuclear explosions on the earth's atmosphere, ionosphere and magnetosphere; effects of electromagnetic and particulate radiations on space systems; space instrumentation; propellant chemistry, chemical dynamics, environmental chemistry, trace detection; atmospheric chemical reactions, atmospheric optics, light scattering, state-specific chemical reactions and radiative signatures of missile plumes, and sensor out-of-field-of-view rejection.

MORE

DISPLAY 02/2/1

96N13856*# ISSUE 2 PAGE 462 CATEGORY 46

RPT#: NASA-CR-199697 NAS 1.26:199697 ATR-94(7251)-1 NIPS-95-05899 CNT#:
NAG5-1100 95/11/01 24 PAGES UNCLASSIFIED DOCUMENT

UTTL: The mosaic structure of plasma bulk flows in the Earth's magnetotail

AUTH: A/ASHOUR-ABDALLA, M.; B/RICHARD, R. L.; C/ZELENYI, L. M.; D/PEROOMIAN,
V.; E/BOSQUED, J. M. PAA: A/(California Univ., Los Angeles, CA.);
B/(California Univ., Los Angeles, CA.); C/(Institute of Space Research,
Moscow, USSR.); E/(Centre d'Etude Spatiale des Rayonnements, Toulouse,
France.)

CORP: Aerospace Corp., El Segundo, CA. CSS: (Inst. of Geophysics and Planetary
Physics.)

SAP: Avail: CASI HC A03/MF A01

CIO: UNITED STATES

MAJS: /*GEOMAGNETIC TAIL/*ION BEAMS/*ION DENSITY (CONCENTRATION)/*
MAGNETOHYDRODYNAMIC FLOW/*PLASMA INTERACTIONS/*PLASMA LAYERS/*THERMAL
ENERGY

MINS: / GEOMAGNETISM/ MAGNETOHYDRODYNAMICS/ SOLAR WIND/ SPATIAL RESOLUTION

ABA: Author

ABS: Moments of plasma distributions observed in the magnetotail vary with
different time scales. In this paper we attempt to explain the observed
variability on intermediate timescales of approximately 10-20 min that
result from the simultaneous energization and spatial structuring of solar

ENTER:

MORE



3 1176 01422 2351

Aerospace Report No.
ATR-94(7251)-1

THE MOSAIC STRUCTURE OF PLASMA BULK FLOWS IN THE EARTH'S MAGNETOTAIL

Prepared by

M. Ashour-Abdalla and R. L. Richard
Institute of Geophysics and Planetary Physics
University of California
Los Angeles, California

L. M. Zelenyi
Space Research Institute
Moscow, Russia

V. Perroomian
Space and Environment Technology Center
Technology Operations
The Aerospace Corporation

and

J. M. Bosqued
Centre d'Etude Spatiale des Rayonnements
Toulouse, France

1 November 1995

Engineering and Technology Group
THE AEROSPACE CORPORATION
El Segundo, CA 90245-4691

Prepared for

NASA
Goddard Space Flight Center
Greenbelt, md 20771

Grant No. NAG5-1100


PUBLIC RELEASE IS AUTHORIZED

N96-13856 #

Intentionally Left Blank

THE MOSAIC STRUCTURE OF PLASMA BULK FLOWS
IN THE EARTH'S MAGNETOTAIL

Prepared

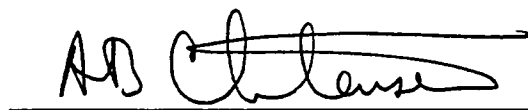


V. Peróomian et al.

Approved



J. B. Blake, Director
Space Sciences Department



A. B. Christensen, Principal Director
Space and Environment Technology
Center

Intentionally Left Blank

Note

The material reproduced in this report originally appeared in *Journal of Geophysical Research*. The ATR is published to document the work for the corporate record.

The mosaic structure of plasma bulk flows in the Earth's magnetotail

M. Ashour-Abdalla,^{1,2} L. M. Zelenyi,³ V. Perroomian,^{1,4} R. L. Richard,¹ and J. M. Bosqued⁵

Abstract. Moments of plasma distributions observed in the magnetotail vary with different time scales. In this paper we attempt to explain the observed variability on intermediate timescales of ~10–20 min that result from the simultaneous energization and spatial structuring of solar wind plasma in the distant magnetotail. These processes stimulate the formation of a system of spatially disjointed, highly accelerated filaments (beamlets) in the tail. We use the results from large-scale kinetic modeling of magnetotail formation from a plasma mantle source to calculate moments of ion distribution functions throughout the tail. Statistical restrictions related to the limited number of particles in our system naturally reduce the spatial resolution of our results, but we show that our model is valid on intermediate spatial scales $\Delta x \times \Delta z \sim 1 R_E \times 1000$ km. For these spatial scales the resulting pattern, which resembles a mosaic, appears to be quite variable. The complexity of the pattern is related to the spatial interference between beamlets accelerated at various locations within the distant tail which mirror in the strong near-Earth magnetic field. Global motion of the magnetotail results in the displacement of spacecraft with respect to this mosaic pattern and can produce variations in all of the moments (especially the x -component of the bulk velocity) on intermediate timescales. The results obtained enable us to view the magnetotail plasma as consisting of two different populations: a tailward-Earthward system of highly accelerated beamlets interfering with each other, and an energized quasithermal population which gradually builds as the Earth is approached. In the near-Earth tail, these populations merge into a hot quasi-isotropic ion population typical of the near-Earth plasma sheet. The transformation of plasma sheet boundary layer (PSBL) beam energy into central plasma sheet (CPS) quasi-thermal energy occurs in the absence of collisions or noise. This paper also clarifies the relationship between the global scale where an MHD description might be appropriate and the lower intermediate scales where MHD fails and large-scale kinetic theory should be used.

1. Introduction

It is generally believed that the transport of magnetic flux, energy, and momentum throughout the solar wind-magnetosphere-ionosphere system can be described in terms of large-scale convection controlled by the magnetospheric electric field. However, observations have shown that the sunward convection flows in the magnetotail which result from this large-scale convection exhibit a great deal of variability, ranging from a few tens of kilometers per second up to ≥ 1000 km/s. This variability has led researchers to conclude that the large-scale convection pattern is highly changeable and distorted and may even be turbulent.

¹Institute of Geophysics and Planetary Physics, University of California, Los Angeles.

²Also at Department of Physics and Astronomy, University of California, Los Angeles.

³Space Research Institute, Moscow, Russia.

⁴Now at Space and Environment Technology Center, The Aerospace Corporation, Los Angeles, California.

⁵Centre d'Etude Spatiale des Rayonnements, Toulouse, France.

During the 1970's the variability of plasma flow in the Earth's plasma sheet on timescales of < 1 hour was studied mainly for geomagnetically disturbed periods [Hones *et al.*, 1972; Hones, and Schindler, 1979; Lui *et al.*, 1977; DeCoster and Frank, 1979]. DeCoster and Frank [1979] used IMP 7 and 8 measurements to show the occurrence of high-speed flows at the boundary of the plasma sheet, moving away from the neutral sheet at 11 km/s. These initial satellite measurements by DeCoster and Frank [1979] showed for the first time that the occurrence of high-speed flows is a spatial rather than a temporal effect. Parks *et al.* [1979] demonstrated that the vertical motion of the plasma sheet has velocities ranging from 10 to 60 km/s. This was later confirmed by Andrews *et al.* [1981], Forbes *et al.* [1981a, b], and Eastman *et al.* [1985]. In addition, Forbes *et al.* [1981a] used two-spacecraft data to show for the first time that the PSBL flows consist of beams with Earthward-flowing plasma near the lobes and beams with tailward (or mixed Earthward/tailward) flowing plasmas nearer the CPS. They found that the highest velocities occur at the outer edges of the PSBL, with lower velocities towards the CPS. A number of studies [Möbius *et al.*, 1980; Andrews *et al.*, 1981; Williams, 1981; Eastman *et al.*, 1984, 1985; Takahashi and Hones, 1988] have established that the PSBL is nearly always present, and velocities as high as 1000 km/s are detected even during quiet times [Takahashi and Hones, 1988]. Takahashi and Hones [1988] estimated that the outermost

Earthward-directed beam was 0.2 to 0.7 R_E thick and found the total PSBL thickness to be substantially more than an Earth radius.

The detailed flow structure of the CPS is not as well known. ISEE observations [Eastman *et al.*, 1985; Huang *et al.*, 1987; Huang and Frank, 1986] show a CPS characterized by isotropic plasma and small flows (< 10 km/s when $AE < 100$ nT). This situation is interrupted by very high-speed flows (> 400 km/s) of short duration during disturbed times [Huang *et al.*, 1987; Ohtani *et al.*, 1992]. Using Active Magnetospheric Particle Tracer Explorer (AMPTE) observations, Baumjohann *et al.* [1989, 1990], and more recently Angelopoulos *et al.* [1992, 1993], also found low-velocity flows (averaging 30–60 km/s) in the CPS. However, although the average velocities they found were quite small, there was a large amount of scatter about the mean velocities. This scatter was interpreted as evidence for the existence of fluctuating electric fields and turbulent transport [Angelopoulos *et al.*, 1993].

Spacecraft usually output data in terms of time series, and although time/space variations cannot be uniquely separated by using data from a single spacecraft, a number of scientists have attempted to use the time series to interpret the observed

variability in the magnetotail flow pattern in terms of temporal effects. The main object of this paper is to present an alternative explanation and show that much of the observed variability on intermediate time scales of ~ 1 –30 min by satellites crossing the PSBL and CPS at $x \sim 10$ –20 R_E (such as ISEE satellites) can be interpreted adequately in terms of spatial structure.

In order to introduce the high variability of the flow in the plasma sheet and particularly the spatial nature of the flow in the PSBL, we start by presenting in Figure 1 a typical example of multiple crossings of the lobe-plasma sheet interface. A number of exit-entry sequences of the ISEE 1 satellite can be seen in this figure in which we plot the moments of the distribution function (obtained every 128 s in the ~ 1 eV to 44 keV range by the University of Iowa LEPDEA instrument) and the electron fluxes at two fixed energies, ~ 1.5 keV and 6 keV, measured simultaneously by ISEE 1 and 2 [Anderson *et al.*, 1978]. Immediately after ~ 1158 UT, ISEE 1 enters the PSBL from the lobe for the first time. This entry is marked by a sharp increase in the plasma density and is characterized by a high-speed flow of ~ 200 –300 km/s directed Earthward and downward for a duration of ~ 10 min, followed by a sequence of small tailward and Earthward flows up to ~ 1215 UT. This enhancement of the bulk

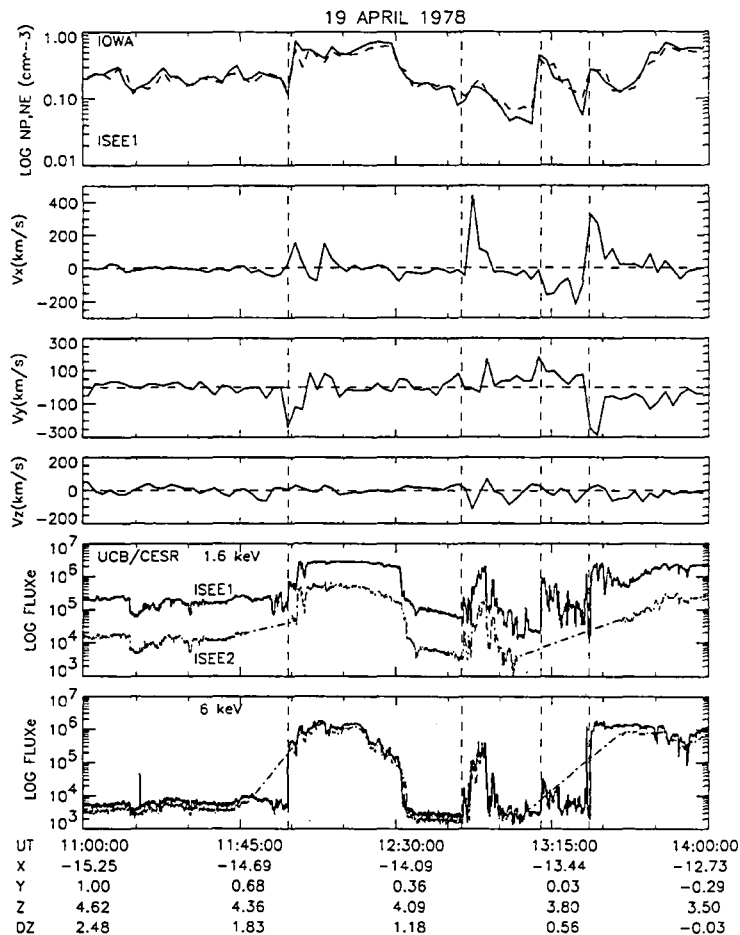


Figure 1. Plasma parameters and electron fluxes from ISEE 1 and 2 satellites, between 1100 and 1400 UT on April 19, 1978. From top to bottom, plasma ion and electron densities, flow velocities (V_x , V_y , V_z) measured by ISEE 1, and 4-s averages of electron fluxes at two fixed energies, ~ 1.6 and ~ 6 keV, measured by ISEE 1 and 2 satellites using GSM coordinates (R_E).

flow is marked by alternate changes in both the v_x and v_y directions. The second brief crossing of the PSBL occurs near ~ 1249 UT, as evidenced by the abrupt increase of the Earthward-directed bulk flow up to ~ 450 km/s; ISEE briefly exits the PSBL (for ~ 10 min) and enters again around ~ 1312 UT. Two consecutive enhancements of the tailward and duskward flow can be detected here. Finally, during the last entry, occurring at ~ 1326 UT, once again a high-speed Earthward flow of ~ 5 – 10 min duration is encountered.

Observations indicate that a majority of the PSBL crossings seen during the 90 min interval were caused by the relative vertical motion of the boundary. High-resolution (4 s) electron fluxes can be used to determine the vertical motion of the boundary. The time delays between the electron profiles at the onset of electron increases were used in conjunction with the known separation distance (~ 150 km in the z direction) between the spacecraft to determine the velocity as being ~ 13 – 20 km/s in the case of the first crossing, occurring around 1200 UT. Assuming that this vertical velocity remains constant during the ~ 1200 – 1215 intervals the thickness of each high-speed flow is of the order of 2300–3600 km. It is important to note here that the detailed ion spectrum between 1159 UT and 1201 UT, during which period the boundary moved ~ 3000 km (see Figure 11a of Parks *et al.* [1984]), is consistent with a mixing of even narrower spatial components of different energies, flowing Earthward and tailward. The second encounter with the PSBL around ~ 1249 UT occurs when the vertical velocity of the tail is much faster, $\sim 48 \pm 15$ km/s, so that the thickness of the outer high-speed beam can be estimated to be $\sim 1 R_E$. At ~ 1326 UT, due to a partial loss of data on ISEE 2, the vertical velocity can only be estimated as being ~ 50 km/s; this corresponds to a vertical extent of $1 R_E$ for the outer beam.

This example clearly shows substructures in the PSBL flow. A crossing of the PSBL (and/or the CPS) that takes 10–30 min, in reality corresponds to a spacecraft having a relative motion through successive and narrow layers with thicknesses ranging from ~ 0.3 to $1 R_E$. On these scales the flow in the outer regions of the plasma sheet appears to be not as well organized and supports frequent changes in amplitude and direction. We refer to this timescale as intermediate because it is lower than MHD spatial and temporal scales but faster than the time scales of typical plasma waves and instabilities.

To investigate the structure of the plasma sheet we carried out a large-scale kinetic (LSK) simulation of magnetotail ion distributions. The main idea of the LSK calculations is to follow the trajectories of noninteracting particles exactly in given realistic \mathbf{B} and \mathbf{E} field models. By recording the position and velocity components of the particles we are able to calculate the distribution function and the resulting moments. Using the Tsyganenko [1989] magnetic field model, a constant dawn-dusk electric field, and assuming a plasma mantle source, Ashour-Abdalla *et al.* [1991a, b; 1993] used LSK to form a plasma sheet populated by hot plasma and composed of a well-defined CPS and PSBL. From these calculations, Ashour-Abdalla *et al.* [1993] studied the microphysics of the magnetotail, including the shape and detailed features of the ion distribution functions. They found intrinsic structures (beamlets) in the distribution functions which they attributed to the nonadiabatic interaction of the plasma with the current sheet. On the global scale, Ashour-Abdalla *et al.* [1994] took moments of the distribution functions throughout the tail and showed that the overall picture obtained agreed with the observed global plasma patterns. In that paper they also showed that although the model used was not self-consistent, ion

distributions in the magnetotail approximately satisfied local stress balance conditions.

In this paper we will go one step further and look at the relationship between the large- and small-scale structures in the tail with emphasis on the structure of the convection system. We find an "intermediate" spatial scale that falls between the large-scale (MHD picture) and the small-scale and is on the order of $1 R_E$ in length and ~ 1000 km in width. This intermediate scale results from the interaction and interference of numerous structures accelerated in different regions of the distant magnetotail. Following this introduction in section 2 we discuss the properties of large-scale flows ($\geq 3 R_E$) and show that in this limit the results agree in general with an MHD approach. As stated above, although we postulate the existence of beamlets [Ashour-Abdalla *et al.*, 1993], we have not discussed their consequences in the magnetotail. We undertake this task in section 3 by first reviewing our understanding of the formation of beamlets and then giving an analytical estimate of the number of beamlets one would expect to see in the chosen magnetotail configuration. In section 3 we also address the natural concern of how these structures survive in the magnetotail after their formation and how long they keep their identity under the influence of numerous effects of smearing and scattering pertinent to the tail conditions. The interference and overlapping of numerous plasma structures accelerated in different regions of the magnetotail leads to the formation of a complicated mosaiclike pattern of plasma bulk parameters. Numerical ramifications of these mosaic structures are presented in section 4. Since the plasma in the tail consists of two populations, one which has suffered a reasonable amount of scattering and one consisting of beamlet particles, we show in section 5 how these two populations coexist and eventually mix. Finally we summarize our results and argue that the basic physics of the tail requires the existence of these spatial structures.

2. Large-Scale Kinetic Modeling and Global Structure of Plasma Flows

2.1. Model

In this paper we use the approach of large-scale kinetics, which has been previously described in detail [Ashour-Abdalla *et al.*, 1993]. In our study we use a two-dimensional (2D) reduction of the Tsyganenko [1989] magnetic field model with an x -type neutral line $100 R_E$ downtail (see Ashour-Abdalla *et al.* [1993] for details) along with a constant, dawn-to-dusk directed convection electric field of 0.1 mV/m, typical for quiet magnetospheric periods. Throughout this paper we assume a coordinate system with z northward, x antisunward, and y toward dawn. In this coordinate system $x = 0$ is at Earth's center, and $z = 0$ coincides with the current sheet plane. The width of the tail in our model is $25 R_E$ with the dawn flank lying at $y = 12.5 R_E$ and the dusk flank of the tail at $y = -12.5 R_E$. The ion sources are located in the plasma mantle at $x = 15 R_E$, $z = \pm 8 R_E$ and extend from $y = -12.5 R_E$ to $y = +12.5$ in $1 R_E$ increments. Because of the small thickness of the plasma mantle, it is a good approximation to neglect its thickness in z . The finite spread would produce a velocity spread during the first crossing that is less than the thermal velocity and much less than the convection velocity in the current sheet. Each source distribution is a drifting Maxwellian with a temperature of 300 eV and a field-aligned bulk flow velocity of 200 km/s. Particles are collected at a series of virtual detectors at various positions in x , y and z . When

particles cross these detectors we record the position and velocities of the particles entering the detectors. We use this information to calculate distribution functions and then compute the bulk flow and other moments.

2.2. Global Structure of Plasma Flows

Before trying to determine the physics of smaller scale ($\leq R_E$) structures of the plasma sheet, it is necessary to first review the large-scale pattern of plasma bulk flows in the magnetotail region.

Figure 2 illustrates the large-scale distribution of plasma bulk flows in the equatorial region of the magnetotail. This plot was obtained by binning the bulk velocities of ions in $3 R_E \times 3 R_E$ x - y bins and averaging to obtain V_x , V_y , and V_z for each bin. Because of symmetry, $V_z = 0$ in this plane. The length of the arrows correspond to the magnitude of the velocity in the plane (scale shown at the top of the figure) and the direction of the arrow gives its angular orientation. As one can see the average flow velocities in the x -direction are Earthward in a large part of the magnetotail, and the typical magnitude of these flows (~ 50 km/s at $x \sim 20 R_E$) corresponds fairly well to the value of the local convection velocity in the x direction $V_c = E_y/B_n(x)$. Closer to the Earth ($x \leq 15 R_E$) the x component of flow becomes very weak, and all flows are predominantly directed duskward. The duskward flow becomes overwhelming near the "wall" region [Ashour-Abdalla et al., 1992] where the magnetic field (and therefore pressure) have strong gradients. The duskward component of the average flow vectors is largest near the duskward flank of the model magnetotail. This average pattern conforms reasonably well with spacecraft data taken in the quiet CPS, especially near the noon-midnight meridian where the results are least influenced by the two-dimensionality of the

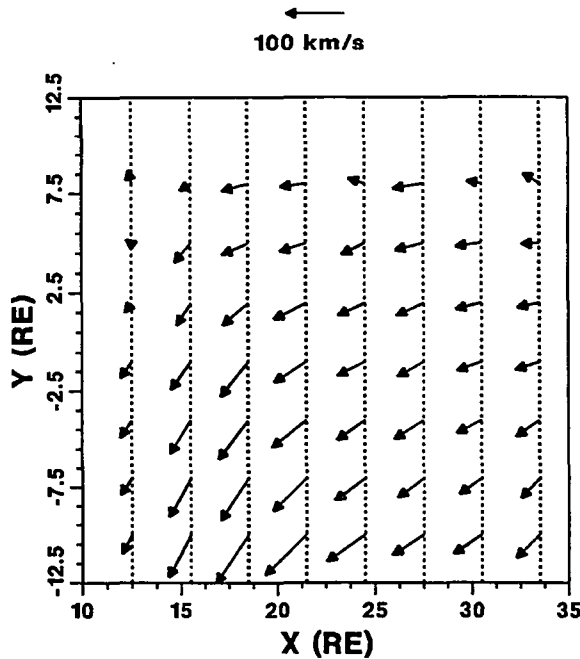


Figure 2. Large-scale bulk flows in the equatorial magnetotail obtained by collecting data in $3 R_E \times 3 R_E$ bins.

model [e.g., Baumjohann et al., 1989; Angelopoulos et al., 1993]. The results shown here are averaged over large spatial bins which correspond to the procedure normally used in statistical analysis of satellite data [e.g., Angelopoulos et al., 1993]. In the next section, in which we deal with local results, we will see how rich in small-scale structure the detailed picture can be in comparison with this MHD-like large-scale pattern. We will also show that the level of variability in the flows ($\Delta V/V$) is much larger than those in the density and pressure distributions.

3. Origin of Beamlet Structure

In the distant tail the conservation of the magnetic moment μ breaks down and ions can no longer be described by guiding center trajectories. The behavior of ions there is principally governed by the parameter of adiabaticity

$$\kappa = (R_{\text{curv}} / \rho_{\text{max}})^{1/2} \quad (1)$$

where R_{curv} is the minimum radius of curvature of field lines achieved at $z = 0$ and ρ_{max} is the maximum value of the ion Larmor radius [Büchner and Zelenyi, 1989]. The parameter of adiabaticity κ can also be written as

$$\hat{\kappa} = \sqrt{\frac{R_{\text{curv}}}{\rho_{\text{max}}}} = \left(\frac{e^2}{2m_i} \right)^{1/4} B_n B_0^{-1/2} L^{1/2} \hat{W}^{-1/4} \quad (2)$$

Equation (2) relates κ with the plasma and magnetic field parameters. Here B_n is the normal magnetic field, B_0 is the lobe magnetic field, \hat{W} is the energy of the particles in the de-Hoffman-Teller frame corresponding to convection of particles in the dawn-dusk electric field E_y , and the circumflex indicates that we define the dimensionless parameters $\hat{\kappa}$ and \hat{W} in a moving frame.

If the local convection velocity $V_c = E_y/B_n(x)$ is small compared to the thermal energy of the particles, then $\hat{W} \approx W$. However, in the distant tail where $B_n(x)$ is small, $V_c \gg V$ and $\hat{W} \approx m_i V_c^2 / 2 \approx m_i E_y^2 / 2 B_n^2(x)$. $\hat{\kappa}$ acquires the approximate form [Ashour-Abdalla et al., 1993]

$$\hat{\kappa} = \left(\frac{e}{m} \right)^{1/2} B_n^{3/2} E^{-1/2} B_0^{-1/2} L^{-1/2} \quad (3)$$

When $\hat{\kappa} < 1$, the Larmor radius is larger than R_{curv} and the guiding center approximation is violated [Büchner and Zelenyi, 1989]. However for $\hat{\kappa} < 1$ the invariant,

$$I_z = \oint V_z dz \quad (4)$$

[see Speiser, 1965; Sonnerup, 1971; Büchner and Zelenyi, 1989] is approximately conserved. In this paper we use I' , which is a normalized dimensionless parameter related to I_z by

$$I' = \frac{3\pi}{8} \left(\frac{e B_0}{L} \right)^{1/2} (2m_i W)^{-3/4} I_z \quad (5)$$

where W is the energy of the particle in the given frame. The role of I' in quasi-adiabatic theory is similar to that of $\bar{\mu} = \mu/\mu_{\text{max}} = \sin^2 \nu$ in guiding center theory (where ν is the pitch angle of the particle) [Büchner and Zelenyi, 1989]. I' also can be written as a function of α_0 and β_0 , the angles of the particle's velocity

vector with respect to the equatorial plane ($z = 0$) during its equatorial crossing [Büchner and Zelenyi, 1989]:

$$I' = \sin^{3/2} \alpha_0 f\left(\sin \frac{\beta_0}{2}\right) \quad (6)$$

where $f(k) = (1-k^2)K(k) + (2k^2-1)E(k)$, and $K(k)$ and $E(k)$ are full elliptical integrals.

For certain values of κ called resonant values (κ_R), I' remains small. Particles with $\kappa \sim \kappa_R$ experience minimum scattering during their interaction with the current sheet. The resonant κ values are given by

$$\frac{C(I')}{\kappa_R} = N + \frac{1}{2} \quad (7)$$

where N is an integer and the function $C(I')$ is given by [Ashour-Abdalla et al., 1993]

$$C(I') = 4\sqrt{\pi} \frac{\Gamma(3/4)}{\Gamma(1/4)} + O(I') \quad (8)$$

The term with I' is small even for $I' \sim 1$, so we can neglect the dependence on I' and use $C(I') = \text{const} = 0.763$. This value is

very close to the numerically obtained $C = 0.8$ [Büchner, 1991] and $C = 0.84$ from a corresponding expression found by Burkhardt and Chen [1991]. For the present discussion it is important that these local conditions be written assuming a local deHoffman-Teller (HT) frame for each interaction. This gives

$$\hat{\kappa}_R = \frac{C}{N+0.5} \quad N=1,2,3,\dots \quad (9)$$

The occurrence of resonances is consistent with the results of Burkhardt et al. [1991], who found fluctuations in density and current resulting from energization during neutral-line reconnection, and with Moses et al. [1993], who found that neutral line acceleration of ions resulted in the formation of bunched distributions. The solid line in Figure 3 is a plot of $\hat{\kappa}(x)$ for the T89 model, with the scale shown on the left of the figure. Using this curve and (9) we can obtain the locations X_N where resonance occurs. Figure 3 also shows the locations of resonance (marked X_1 – X_7) and the regions of maximum trapping (marked X_2^* – X_6^*). The energy of the particles accelerated at each resonance location according to $\Delta W \rightarrow 2mV_c^2(x)$ is also shown (dashed curve), with the scale on the right of the figure. We refer to each substructure accelerated at a given resonance N as beamlet number N . The total number of beamlets is limited because higher order resonances overlap and are smeared into one.

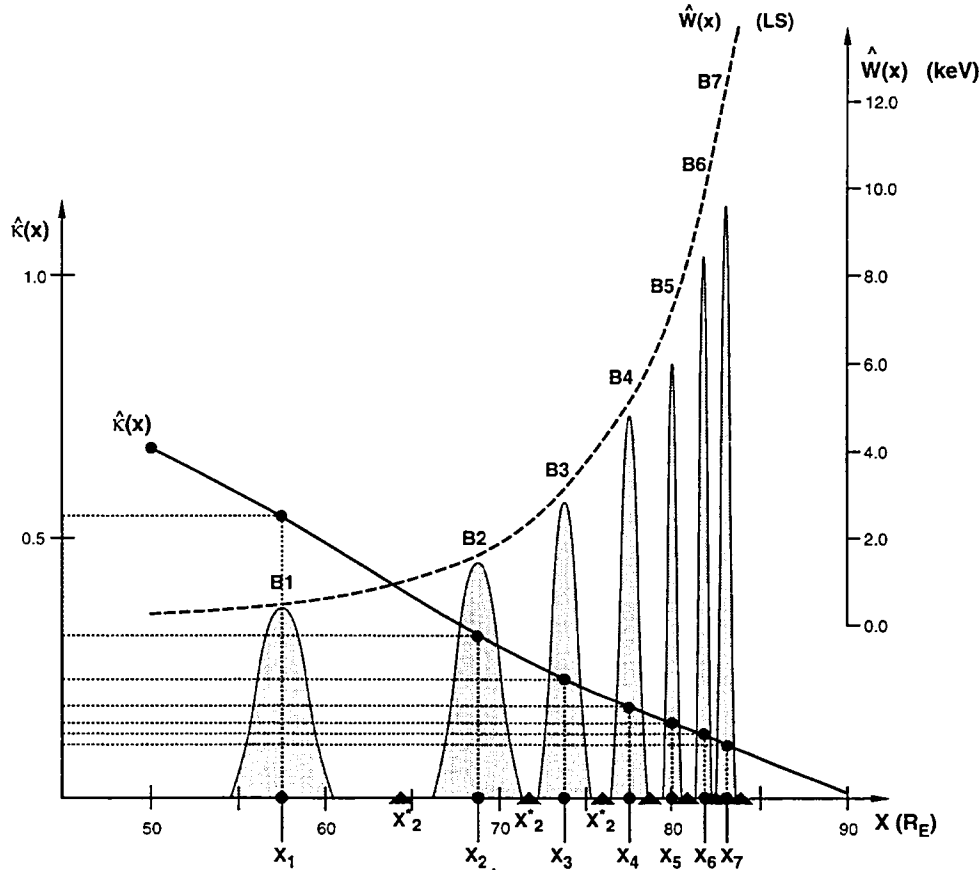


Figure 3. Schematic showing $\hat{\kappa}(x)$ (solid line, scale shown on left of figure) calculated for the T89 model, and $\hat{W}(x)$ from Lyons and Speiser, [1982] (dashed line, scale on right). The locations of resonance regions (X_1 – X_7) are shown with particle distributions; the maximum trapping regions (X_2^* – X_6^*) are marked on the horizontal axis.

Let us now estimate the maximum number of resonances that might be obtained in a given magnetic field. The field reversal region of the magnetotail can be characterized by two main parameters: the thickness of the region, L (which is assumed to be constant in the T89 model), and the magnetic field component normal to the current sheet plane ($B_n(x)$). Since the model contains a neutral line at $X_N = 100 R_E$, $B_n(x)$ can be approximated by a power law dependence over the large region of the tail extending from $x \sim 40$ to $100 R_E$:

$$B_n(x) = B_{np} \left(\frac{X_N - x}{X_N - X_p} \right)^q \quad (10)$$

where $B_{np} = B(X_p = 40 R_E)$ corresponds to the value of $B(x)$ at $X_p = 40 R_E$. For the T89 model, $B_{np} \approx 1.4$ nT and $q = 1.59$.

Higher order resonances occur in the region of small $\hat{\kappa}$, where the Larmor radius of the particles in the current sheet plane becomes larger. This provides a natural thickness for the resonance. Thus we assume that the resonances will overlap if

$$X_N - X_{N-1} = \hat{\rho} = \frac{\hat{V}}{\Omega_n(X_N^*)} \quad (11)$$

where \hat{V} is the velocity and Ω_n is the gyrofrequency at a point between the resonance positions. Here we consider the problem again in the local HT frame and estimate $\hat{\rho}$ at some intermediate point X_N^* between resonances number N and $N - 1$

$$\hat{\kappa}(X_N) = \frac{C}{N + 1/2} \quad (12a)$$

$$\hat{\kappa}(X_{N-1}) = \frac{C}{N - 1/2} \quad (12b)$$

$$\hat{\kappa}(X_N^*) = \frac{C}{N} \quad (12c)$$

The position X_N^* is chosen rather arbitrarily but the exact position of X_N^* has only a minor influence on the final results. The main variation in $\hat{\kappa}(x)$ in both the (2) and the (3) regimes comes from the variation of $B_n(x)$, so below we assume that the other parameters (B_0 , L) in the definition of $\hat{\kappa}$ are constant.

Let us start with the case $E_y = 0$ (or $V > V_c(x)$), which is the case for the $N = 1$ and $N = 2$ resonances in our model. From (2), (11) and (12) we obtain for the magnetic field profile approximated by (10):

$$N_{\max} = \left(\frac{X_N - X_p}{\sqrt{L\rho_0}} \right)^{\frac{q}{2q+1}} \frac{1}{\kappa_p^{1/2q+1}} \frac{C^{\frac{q+1}{2q+1}}}{q^{\frac{q}{2q+1}}}, \quad (13)$$

$$E = 0, \text{ or } V \gg V_c(x)$$

Here ρ_0 is the Larmor radius of ions in the field B_0 and $(L\rho_0)^{1/2}$ is the thickness of the meandering region. For our model we estimate $X_N - X_p \sim 60 R_E$, $(L\rho_0)^{1/2} = 0.5 R_E$, and $\kappa_p \sim 0.7$, and for $C = 0.76$, $q = 1.5$, we get $N_{\max} \sim 7$.

This calculation overestimates the number of beamlets because it neglects the additional smearing related to convection. In the

region of overlapping higher-order resonances the effective Larmor radius significantly enhances $\hat{\rho} = [E/B_n(x)]/[eB_n(x)/m_i]$ due to the presence of this convective electric field, and this should influence the overlapping of neighboring resonances. However the values of $\hat{\kappa}$ and κ decrease simultaneously as a result of the increase in E_y . Therefore the final result is not easy to predict.

If we perform a transformation to the local HT frame and assume for simplicity that $V_c(x) > V_0$ (i.e., $\hat{\kappa}(x)$ is described by (3) we again get from (11) and (12) the expression for N_{\max} :

$$N_{\max} = \left(\frac{X_N - X_p}{L} \right)^{\frac{3q}{7q+2}} \left(\frac{B_0}{B_p} \right)^{\frac{3q}{7q+2}} \left(\frac{L}{\rho_\infty} \right)^{\frac{q-1}{7q+2}} \left(\frac{2}{3q} \right)^{\frac{3q}{7q+2}} \frac{4q+2}{C^{7q+2}}$$

$$E \neq 0, \text{ or } V_c(x) \gg V \quad (14)$$

Here we have the same parameters as in (13), except that $\rho_\infty = (E, B_0)/(eB_0, L)$ is the Larmor radius in the B_0 field based on the convection velocity in lobe region. All terms except the first are very close to 1. Estimating N_{\max} for $X_N - X_p \sim 60 R_E$ and $L \sim 1 R_E$, gives

$$N_{\max}^{E \neq 0} \sim \left(\frac{X_N - X_L}{L} \right)^{9/25} \sim 60^{9/25} \sim 4 - 5 \quad (15)$$

As one can see from (14), $N_{\max}^{E \neq 0}$ includes a very weak dependence on E given by

$$N_{\max}^{E \neq 0} \sim E^{(1-q)/(7q+2)} \sim E^{-1/25}$$

This weak dependence means that the effects of the increase of $\hat{\rho}$ (which enhances the overlapping) and the reduction of $\hat{\kappa}$ (which makes the separation between resonances larger) almost compensate each other. It is interesting to note that for the weak dependence of $B_n(x)$ on x , when $q < 1$, the number of structures could even grow with an increasing E .

With the assumption $V_c(x) > V_0$ the energy of each beamlet can be estimated,

$$V(X_N) \sim 2 V_c(X_N)$$

$$W_{bN} = \frac{m_i V^2(X_N)}{2} = 2(N + 0.5)^{4/3} \left(\frac{E}{B_0} \right)^2 \left(\frac{L}{\rho_\infty} \right)^{2/3} \quad (16)$$

One very important point in the comparison of our results with those obtained by Huang *et al.* [1987] and Burkhardt and Chen [1991] is that they considered the one-dimensional current sheet to have a fixed B_n so that in a resonant condition like that in (7) the only parameter they could vary was energy. There is no fundamental disagreement in the general physics of our results because, as we have shown above, even the numerical value of the resonant parameter κ_R could be reproduced with very good accuracy by using separatrix theory. The principal difference is in the application to the real magnetotail with its convection electric field. The energy of the particles interacting with the current sheet in the regions of effective acceleration [$m_i V_c^2(x)/2$] is determined by the convection velocity, and is not a free parameter that can be varied arbitrarily. Formally it can be

defined as the difference between the usual energy dependent $\kappa(W, B_n)$ defined by (2) and the $\hat{\kappa}$ defined by (3), which is already energy independent and which should be used for regions in which accelerated structures occur. The structures we expect to obtain in the tail are spatial, not structures in velocity space, as was suggested by *Huang et al.* [1987]. Analytical theory predicts that the combined processes of acceleration and structuring which take place during the interaction of particles with the current sheet produces a finite number (4–6) of strongly accelerated ion beams highly collimated along field lines. Particles accelerated at locations in between resonances are scattered and form a second plasma population with distinct properties.

Analytical theory has limited applications in modeling a realistic tail (even 2D) because many simplifying assumptions are needed to reach analytically tractable results. The parameter κ is usually not small enough for the assumptions we have used to be valid in the main part of the tail: κ becomes greater than 1 as Earth is approached, so the diffusion-like picture based on small jumps of $\Delta I_z/I_z \ll 1$ usually fails for large regions of the tail. Thus the use of numerical techniques is unavoidable in analyzing this problem. Because the primary acceleration occurs in a region where B_n and the corresponding κ remain small, analytical theory generalized to include the effects of convection and the gradients of tail parameters in x can be used as a guide to interpret modeling results. It is clear that because of the considerable number of simplifications made in setting up the analytical theory, one should practice caution when comparing the analytical and the numerical results.

4. Propagation and Interference Pattern of Beamlets

4.1. Propagation of Beamlet Particles

In this section we consider what happens to the structures (beamlets) after their formation at the X_N ($N = 1, 2, \dots, 5$) locations in the distant tail. Each of these beamlets has a different velocity (16), and during propagation to Earth they experience $\mathbf{E} \times \mathbf{B}$ drift in the lobe ($\sim B_0$) magnetic field. The velocity filter effect [*Green and Horwitz*, 1986; *Liu and Hill*, 1986] influences their distribution in space in the course of their Earthward propagation. In Appendix 1 of *Ashour-Abdalla et al.* [1993] this problem was analyzed for the simplified model $\mathbf{B} = B_0 \frac{z}{L} \mathbf{e}_x + B_n(x, z) \mathbf{e}_z$, and it was shown that the velocity filter effect can result in an increased separation of beamlets with distance. Although in a realistic magnetic field model the distance will diminish due to convergence of field lines, the result is still valid that beamlets maintain their identities while propagating towards Earth (see (A8)–(A9) from *Ashour-Abdalla et al.* [1993]). Near Earth some beamlet particles are precipitated and others are reflected. Precipitated beamlet particles manifest themselves as velocity dispersed ion structures (VDIS) [*Bosqued*, 1987; *Zelenyi et al.*, 1990; *Ashour-Abdalla et al.*, 1992; *Bosqued et al.*, 1993] characterized by a latitude-energy dispersion consistent with distant tail beamlet acceleration (higher energies at higher latitudes).

Nonprecipitating beamlet particles form a tailward-propagating beam, which in turn interacts with the current sheet and can be accelerated again in the manner discussed above. It is unlikely that this beam will hit the current sheet at another resonance location X_k , and therefore after this and subsequent interactions with the current sheet it will gradually be scattered

into the quasi-isotropic population (see section 5). Although some elements of this process could still be described analytically the picture becomes increasingly complicated and to understand it we should return to numerical results.

Plate 1 shows the trajectories of one particle from each beamlet and illustrates this pattern. As we will see below (section 5), the beamlet particles move as a group and do not diverge in space for a relatively long time. Although individual beamlets remain distinct, near-Earth reflection causes Earthward- and tailward-moving beamlets to intersect each other throughout the magnetotail. In the next subsection we discuss the consequences of the interference of beamlets.

4.2. Interference of Streaming and Counterstreaming Beamlets

As we saw in Plate 1, multiple Earthward-moving beamlets should intersect with the tailward parts of the other beamlets. If we assume (and the assumption is supported by modeling results) that the beamlets retain their identity after at least two interactions with the current sheet (they may do so even longer), then we will have about $2N_{\max}$ tailward-moving and $2N_{\max}$ Earthward-moving filaments. Taking into account that the Earthward-moving part of the outermost beamlet does not intersect any returning beams, we can estimate that the number of such intersections in the northern hemisphere is about $(2N_{\max}-1)^2 \sim 80$. This rough estimate gives the impression that the appearance of such interference regions (about 100–200 of them) is a common feature of the magnetotail. One such interference region is identified in Plate 1 (box at $x \sim 40 R_E$, $z \sim 4 R_E$).

The velocity dispersion of PSBL beams is such that beam velocities are higher at higher z [e.g., *Forbes et al.*, 1981a; *Takahashi and Hones*, 1988]. At the same time, convection moves reflected beams to a lower z than the Earthward-directed beams. As a beamlet moves Earthward or tailward it ($\mathbf{E} \times \mathbf{B}$) convects toward the neutral sheet. A tailward-moving (reflected) beamlet may therefore intersect the adjacent Earthward-moving (original) beamlet. Assuming that the beamlets have approximately the same density, the net effect at an intersection (illustrated schematically in Figure 4) is a small but tailward directed bulk velocity. Each beamlet actually has a smooth profile $n(z)$, and Figure 4 is highly simplified. Actually beamlets are spatial structures that have a density maximum in their centers. Positive and negative density gradients occurring at the edges of beamlets result in a magnetization current.

At interference regions, together with compensation for net bulk flow, one should see an enhanced (approximately doubled) plasma density that results from the overlapping of beamlets. This effect might be related to the experimental finding by *Baumjohann et al.* [1990] of an anticorrelation of bulk velocity and density in the PSBL. Each local enhancement of density (and therefore of pressure) should also result in peaks of V_y where there are sharp local density gradients produced as a result of this interference.

We illustrate the interference of beamlets in the x - z plane in Figure 5. This figure is a schematic representation of an interference region (shown with box in Plate 1) and shows an Earthward propagating beamlet (beamlet ($k - 1$)) interfering with the reflected portion of beamlet k . Since beamlets in the PSBL and outer CPS (OCPS) are predominantly field-aligned and have a relatively small convection velocity, their interference should occur at small angles resulting in overlapping regions being long (in x) in comparison with the thickness of the beamlets them-

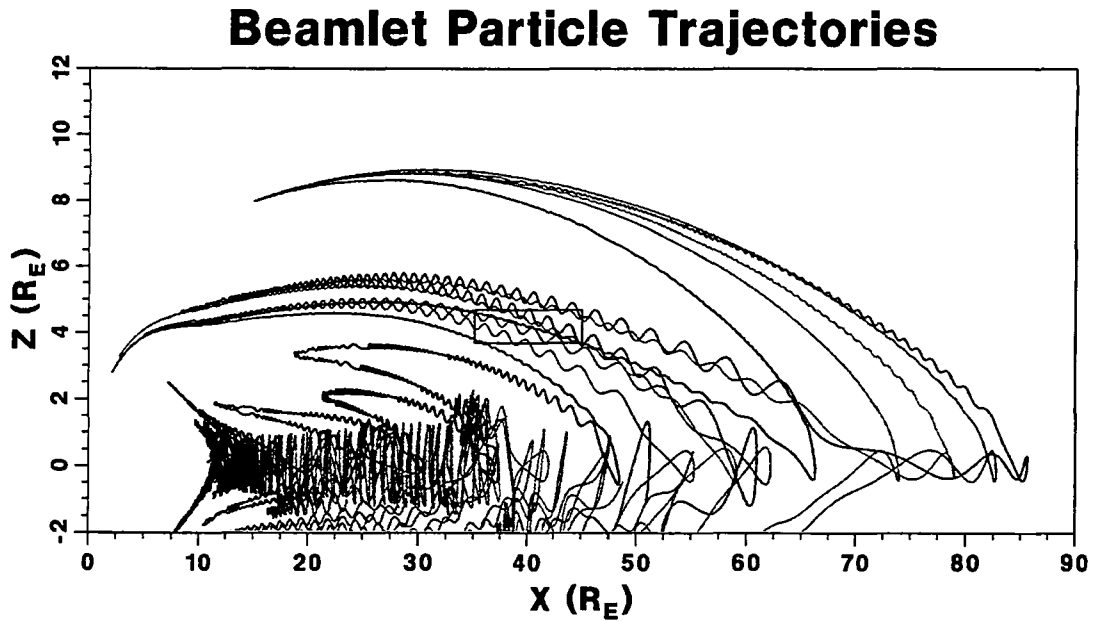


Plate 1. Trajectories of five beamlet particles launched from the plasma mantle projected onto the x - z plane. Rectangular box denotes interference region.

selves (in z). It is clear from this schematic that the dimension in z , Δz , is simply due to the spatial extent of the beamlet whereas the dimension in x , Δx , results from the interference of beamlets. This interference pattern of beamlets leads to structuring on an "intermediate" scale. The intermediate scale is $\Delta x \sim 1 R_E$, $\Delta z \sim 1000$ km.

As discussed above, a number of unusual effects appear within these regions, which can be well within the PSBL or the OCPs, such as a dramatic decrease of bulk velocity, an increase of density, localized peaks of V_y , and variations in the B_x magnetic field due to enhanced pressure. The occurrence of such rapid changes in a dense region without large bulk flows could be misinterpreted, for example, as exits from the PSBL or different plasma clouds [e.g., Belova *et al.*, 1987]. The beamlet interference region has two counterstreaming populations, a situation that is very unstable to the generation of a number of instabilities, especially broadband electrostatic noise (BEN) [Schrifer and Ashour-Abdalla, 1990, 1991]. We might expect that regions of enhanced BEN would have a mosaiclike or patchy pattern in the PSBL.

4.3. Magnetotail Plasma Flows

As we argued in the preceding subsection, interference of multiple beam structures should result in a complicated patchy or mosaiclike pattern of plasma distributions in the magnetotail. Elements of this mosaic could be as small as the thickness of beamlets and therefore should scale as fractions of R_E (say 1000 – 2000 km). In previous publications we used virtual detectors at planes of constant x and interpolated to obtain an average pattern of plasma moments in the x - z plane [Ashour-Abdalla *et al.*, 1993, 1994]. Although this method provided very convincing evidence of structuring along the z axis, the use of interpolation between detectors placed several R_E apart smeared all of the small-scale effects. The advantage of using x detectors was that we averaged

numerical data in the y direction, thus improving our statistics and could prove the existence of beamlets.

To identify the fine-scale pattern in meridional planes without large-scale averaging we used a detector along the noon-midnight meridian ($y = 0$). This provided high spatial resolution of our structures, at the cost of poorer statistical results. The total number of particles in the simulation plays an important role in improving the results so that they are statistically reliable. Using only 100,000 or even 200,000 particles, we found large variations in the moment values in each bin. These values rapidly converged for results calculated with 300,000 or more particles in

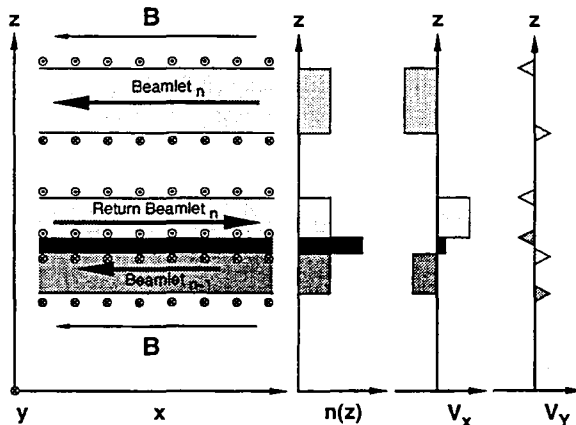


Figure 4. Schematic of a cut at a $x = \text{const.}$ plane, showing the flows generated at the edges of beamlets (left-hand panel), the increase in local density (second panel from left), change in V_x (third panel), and intermittency of V_y (fourth panel) caused by the overlapping of beamlets.

the system. Figure 6 is a plot of V_x , V_y , and n as a function of x for different total numbers of particles in the calculations. Here we show results for 300,000 particles (dotted curve), 400,000 particles (dashed curve) and 500,000 particles (solid curve). We see that the results for all three cases are virtually identical and the intermediate scale emerges explicitly. In this particular case ($z = 0$) we find $\Delta x = 2 R_E$, which is equivalent to several bins in x . To be able to resolve the intermediate scale, we require a bin size several times smaller than Δx . In order to have statistically meaningful results, we use 500,000 particles in our simulation.

Plate 2a shows the density distribution in the $y = 0$ plane. On a large scale, the features of this pattern resemble those seen in our previous published work [Ashour-Abdalla et al., 1994, Plate 2] but the fine-scale structure is new and difficult to predict. On a smaller scale one would expect that beamlets in general and overlapping beamlets in particular would result in regions of enhanced density. In the PSBL there are localized, sharp-edged density dropouts and increases, and this structuring is especially pronounced in the distant tail. This intermittency is manifested not only in the PSBL, but also, surprisingly, in the CPS and even in the current sheet near $z = 0$. After reflection in a stronger field near the Earth, beamlets supply an enhanced particle flux to certain locations in the CPS in addition to the quasi-isotropic scattered population from ions trapped in the CPS. Beamlets arriving in the current sheet cause regions of enhanced density, and when they leave for the PSBL there are density dropouts. On a larger scale there is a large density dropout in the CPS near $x = 60 R_E$, a position too far Earthward to be populated by particles from the mantle and too far tailward for particles leaving the CPS at larger x to form beamlets to have returned. The picture also shows a clear transition from a thin to a thick plasma sheet at near $x = 70 R_E$.

The most surprising structures in Plate 2 are in the velocity profiles. The component of bulk velocity in the x -direction ($V_x(x,z)$) (Plate 2b) shows how variable and patchy the pattern of bulk flows in the magnetotail can be even for quiet times. One exception is the outermost edge of the PSBL, where the most

highly accelerated particles are found. This large outermost Earthward beamlet does not experience interference from other beamlets and has a strong Earthward bulk velocity streaming with $V \geq 700$ km. The ISEE results [Forbes et al., 1981a; Takahashi and Hones, 1988] have shown that the highest speed Earthward beam is effectively the first seen when entering the surface layer of the PSBL from the lobe and is a characteristic signature of the PSBL. The pattern in this plate is even more patchy than that for density, because we have mixed regions of strongly negative (Earthward flow, blue), strongly positive (tailward flow, yellow) and small bulk velocities (when oppositely directed beams superpose, purple). We see the manifestations of distinct beamlets as well as the regions of overlapping beamlets. The small scale size of the elements of this mosaic, sometimes less than $1 R_E$ across, yield up to several tens of individual elements. The intermittency of bulk flow velocities is astonishing but is not due to numerical and/or statistical effects; instead it is the result of the physical picture described above. We can easily foresee that a spacecraft engulfed by this mosaiclike external plasma sheet will detect alternate sheets of Earthward/tailward flows as shown in the experimental example of Figure 1.

Plate 2c shows the distribution of duskward and dawnward $V_y(x,z)$ components of the bulk velocity. This pattern is different from that for V_x or density as the scale of the patches is smaller than for the $n(x,z)$ or the $V_x(x,z)$ pattern. The spikes in V_y should result from ion gyroradius effects at the edge of each beamlet in which there is a local peak in density, and they should occur twice as often as the local density peaks. These duskward flows are important even though they are small in comparison with the V_x flows in the PSBL, because they can become the dominant component of flow deeper in the CPS where V_x is small on average. Another interesting feature of the $V_y(x,z)$ pattern is the very distinct diamagnetic effect occurring in a very narrow strip at the outermost edge of the PSBL, that is, at the edge of the strongest Earthward beamlet where there is a large gradient in density. Here the duskward flow occurs because of the

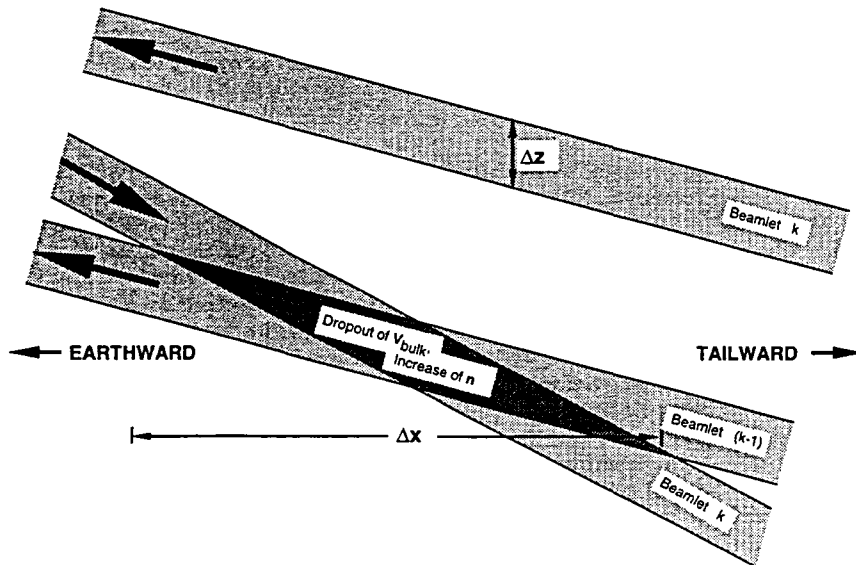


Figure 5. Schematic of beamlet interference representing the area in the rectangular box shown in Plate 1. In this picture $\Delta x \sim R_E$ and $\Delta z \sim 1000$ km.

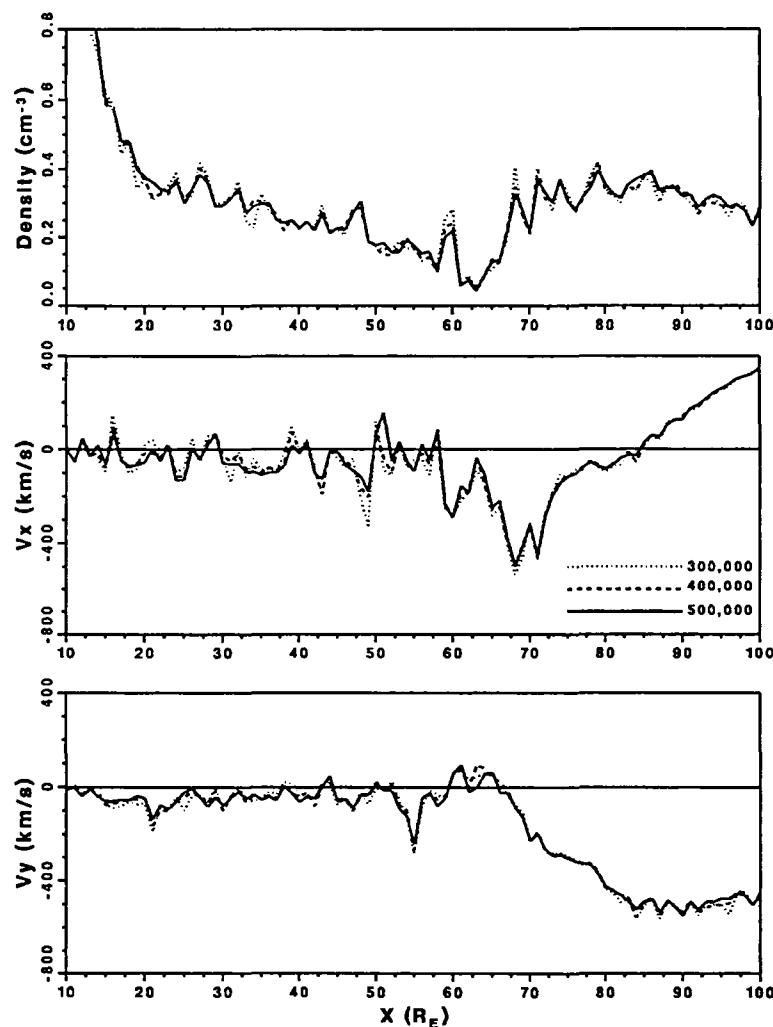


Figure 6. Comparison of moments at $y = 0$ for runs with 300,000 particles (dotted line), 400,000 particles (dashed line), and 500,000 particles (solid line). (Top panel) density profiles, (middle panel) x component of bulk velocity, (bottom panel) y component of bulk velocity.

noncompensated ion gyration in this beamlet. Its thickness can be used to estimate the density gradients between the PSBL and the tail lobes.

We will now explain a large-scale feature evident in Plate 2, but not manifested in our previous results. This is a throatlike transition from a thin plasma sheet to a thick one occurring in Plates 2a–2c at $x = 65 R_E$ which shows a strong dominant duskward velocity at large x (Plate 2c) and a reversal in the V_x -velocity at $x = 80 R_E$, as shown in Plate 2b. The schematic shown in the top panel of Plate 3 illustrates that in the distant tail where the primary acceleration takes place, particles traverse very large distances across the current sheet in a meandering mode of motion when they are trapped within the region. Because the gyration of meandering ions near $z = 0$ is directed duskward in the current sheet, we see strong duskward V_y flow in this region.

The position of the throat (at $x = 65 R_E$), that is, the location where the blue (Earthward) beam starts to emerge from the current sheet in Plate 2b, can be understood from the following considerations. In order for particles to leave the current sheet

plane at $y = 0$, they must complete their roughly semicircular rotation in the equatorial magnetic field, that is, $2\beta(x_{\text{entry}}) < 12.5 R_E$ where x_{entry} is the x location at which the ion enters the current sheet. Particles entering the current sheet beyond the region where the condition can be met do not become beamlet particles at $y = 0$. Particles that meet this condition can cross the $y = 0$ detector as beamlet particles, but only at lower x , because during their gyration in the B_n field fast convection (large E/B_n) will bring them to significantly smaller $\Delta x = x_{\text{entry}} - x_{\text{exit}} \sim (E/B_n)/(\pi/\Omega_n)|_{x=x_{\text{exit}}}$. The reversal in V_x flow, as one can see from Plate 2b for $y = 0$ occurs at $x = 80 R_E$, that is, at larger distances than the "throat," but significantly closer to Earth than the position of the X line. As one can see in the bottom panel of Plate 3, a plot of the x component of bulk velocity in the $z = 0$ plane, the position of the reversal (visible as a black line between orange and blue areas), has the same value ($x \sim 80 R_E$) at $y = 0$, but its location moves tailward in the $-y$ direction. Near the dusk flank more meandering particles exit from the current sheet because the room for their gyration near $z = 0$ is larger and the

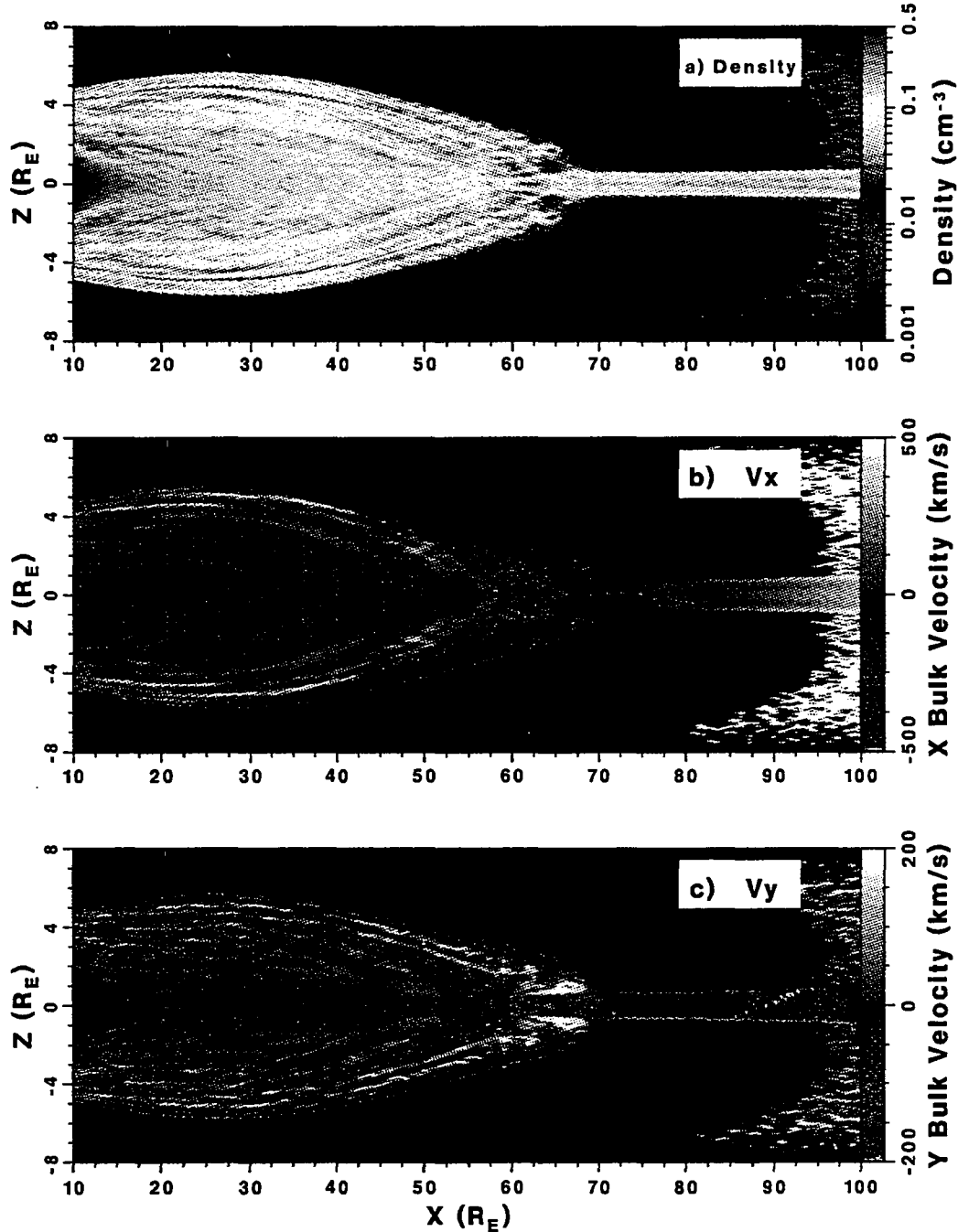
Magnetotail Moment Profile in the Noon-Midnight Meridian

Plate 2. Moments of the distribution function in the $y=0$ plane (noon-midnight) obtained by collecting plasma data in 5800×500 km bins. (a) For the density plot the color coding extends from 0.0 (blue) to 0.6 cm^{-3} (red) on a linear scale. (b) For the x component of the bulk velocity the color coding extends from -500 (yellow) to +500 (blue) km/s . (c) For the y component of the velocity the color coding extends from -200 (yellow) to +200 (blue) km/s .

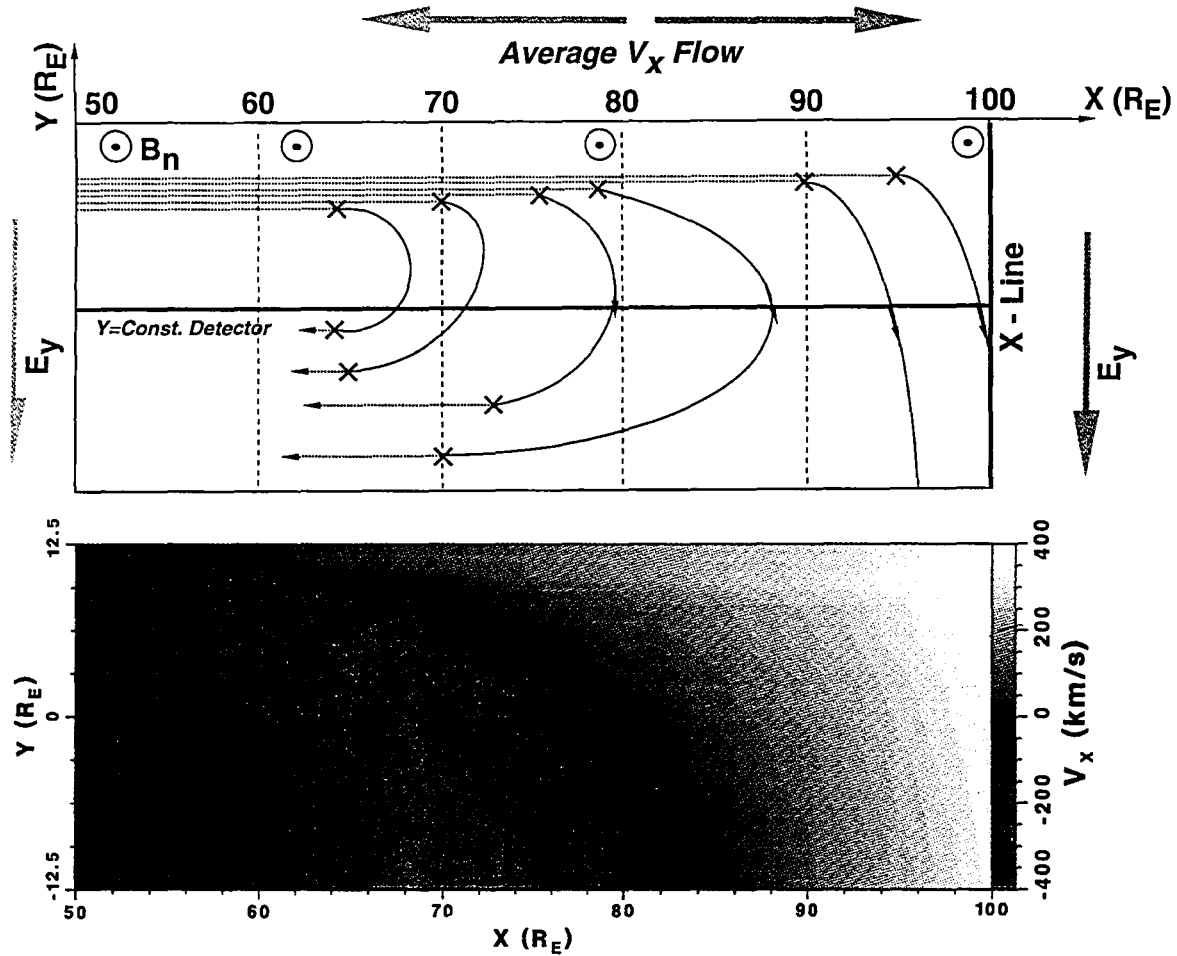


Plate 3. (top) Schematic of ion interactions with the current sheet showing the y extent and turning points of Speiser particles as functions of x . (bottom) The x component of bulk velocity in the $z = 0$ plane showing the location of the flow reversal (black line). Note that although the location of the flow reversal moves tailward toward dusk it is always well Earthward of the X line at $100 R_E$.

reversal in V_x shifts to larger x toward dusk. In the vicinity of the X line, particles have such a large \hat{p} that they move roughly in the $-y$ direction and the bulk flow is determined by incoming tailward moving mantle particles and is directed tailward. The result is a reversal of the bulk flow velocity well Earthward of the nominal position of the X line ($100 R_E$ in our model). This may shed light on some controversies in interpreting ISEE 3 plasma and magnetic field data which give different locations for the distant tail neutral line from plasma and magnetic field measurements. Our point is that due to nonadiabatic ion orbits, these locations of the flow reversal and the $B_n(x)$ reversal should not coincide.

Despite the fact that we used a 2D magnetic field model, the plasma distributions we obtained have an appreciable y dependence, and the pattern obtained at another y detector might be quantitatively different from that shown above, although the main features we observe at $y = 0 R_E$ should appear in a wide range of y values. The pattern we get at more duskward y values ($y < 0 R_E$) might be even more complex because the fastest beamlets moving in the PSBL have access to this detector (acceleration is equivalent to displacement in y in our model). On the other hand,

the dawnside, which is populated with less energetic plasma (i.e., with fewer beamlets), should be less structured and might look more homogeneous. In the last section of this paper we will show some initial results of three-dimensional (3D) modeling and demonstrate that a mosaiclike pattern of magnetotail bulk parameters exists in a 3D system as well as in a 2D system, and therefore is not an artifact of the two-dimensionality of the model discussed thus far.

5. Coexistence and Transformations of Chaotic and Regular Populations in the Magnetotail

The results of 1D models used by *Chen and Palmadesso* [1986] and *Büchner and Zelenyi* [1986] that have been used to chart the development of chaos in a Hamiltonian system cannot be automatically applied to the realistic magnetotail. These models assume that there is unlimited time for the evolution of the system. However, as we have argued in a previous publication [*Ashour-Abdalla et al.*, 1991b], the presence of even a weak convection electric field limits the number of interactions

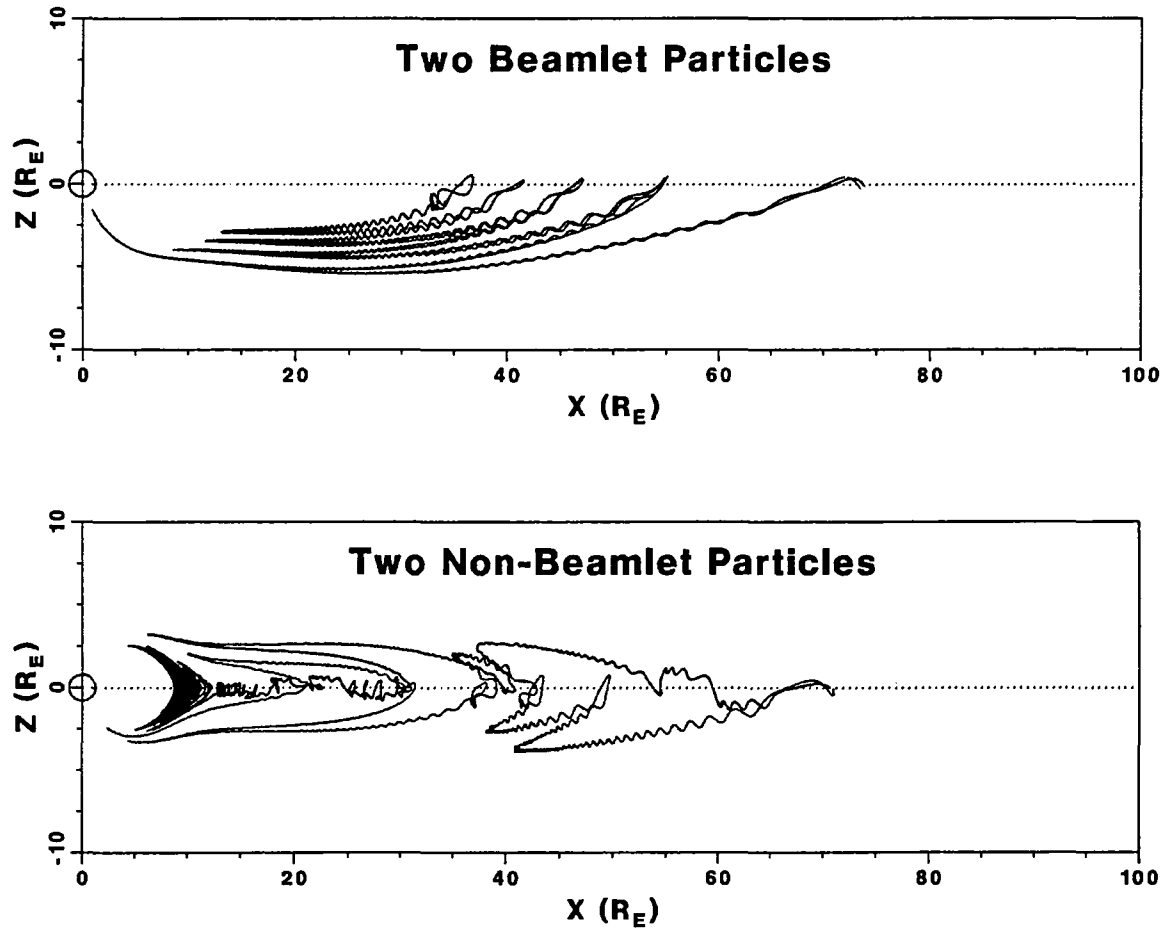


Plate 4. (top) The x - z projections of the trajectories of two beamlet particles. (bottom) Trajectories of two nonbeamlet particles. The pairs of particles are initially $0.1 R_E$ apart in the $z = 0$ plane.

of particles with the current sheet in the $\hat{K} < 1$ region and therefore hinders the development of chaos in the system. In this section we concentrate on the basic interaction of ions with the current sheet and delineate differences in ion behavior that come about because of local parameters of the current sheet where the first interaction occurs. These interactions are important because there are very few resonant positions of scattering in I' and an interaction that occurs between these positions could produce a large scatter in I' . Thus it is possible to be very specific in speaking about the chaotization of ions in the magnetotail.

A well-known quantitative characteristic of chaotic behavior is the Lyapunov exponent. This method was successfully used by Martin [1986] to describe the chaotization near the X line. The Lyapunov exponent (λ) gives the divergence of trajectories in phase space with time as

$$|\Delta d(t)| = |\Delta d_0| \exp(\lambda t) \quad (17)$$

where Δd_0 is the distance in phase space between two neighboring particles at an initial moment and $|\Delta d(t)|$ is the change of this distance with time. For particles on neighboring integrable orbits this parameter should remain very small, since $|\Delta d(t)| \sim |\Delta d_0|$, while for particles on chaotic trajectories (i.e., those

sensitive to initial conditions) it is the rate of their divergence.

Plate 4 illustrates the difference between the properties of particles accelerated at a "resonant" location (i.e., beamlet particles) and those of particles accelerated in the gaps between them. The top panel of Plate 4 shows the x - z projection of the orbits of two beamlet particles. One particle in this panel is colored red, and the second particle is colored blue. Both ions are launched from the plasma mantle and cross the current sheet with a separation of $0.1 R_E$ (initial points are shown in the top panel of Plate 4). This plot clearly shows that the beamlet ions follow very similar trajectories for a long period of time. The lower panel in Plate 4 shows the x - z projection of the orbits of two ions incident on the current sheet at a nonresonant location where maximum scattering is expected. Starting with an initial separation of $\sim 0.1 R_E$, the nonbeamlet ions quickly diverge in space. We can therefore conclude qualitatively that beamlet ions stay together and are capable of traveling in a coherent bunch to the PSBL, while nonbeamlet ions are trapped in the CPS, are scattered and quickly diverge in space.

To make the preceding argument more quantitative, we calculated the parameter λ in (17) by considering the spatial separation of the pairs of particles as a function of time. The results of this calculation are shown in Figure 7, where λ is

plotted as a function of time. We see that for the beamlet particles λ is more than 1 order of magnitude less than that for the pair of nonbeamlet particles, that is, the nonbeamlet particles diverge at a much faster rate than the beamlet ions. For large times, both pairs of ions approach Earth, and the separation distances become small because of the compression of magnetic field lines. Although λ calculated by such a method is not exactly the classic value of the Lyapunov exponent (our λ is for divergence only in geometrical space), it has a similar physical meaning. So we see that due to nonmonotonic properties of particles scattering in the tail, two distinct accelerated populations form during the first interaction of the mantle ion flow (which can also be considered a "coherent" stream) with the current sheet. Accordingly, the destiny of these two populations will be quite different. Scattered ions (which comprise the chaotic part of plasma population) have a sufficiently large I' value to be trapped in the vicinity of the current sheet on short cucumber-shaped orbits and convect towards Earth, and one may speculate that the behavior of this part of the population might resemble that indicated by MHD analysis (we do not attempt to construct a rigorous proof of this speculation). Moreover as the period of quasiadiabatic orbits scales as $(I')^{-2}$ [e.g., Büchner and Zelenyi, 1989], initially scattered orbits with large values of I' have smaller orbital periods, and these ions interact with the current sheet much more often during their Earthward convection than do beamlet particles. This again enhances their scattering, and this part of the distribution becomes rather quickly randomized over the angles. The situation with this part of the distribution is analogous to the evolution of the distribution of guiding center particles experiencing scattering in pitch angles. Since pitch angle diffusion tends to restore the angular symmetry of the distribution by making it isotropic, one could argue that the same effect should produce scattering over the values of I' . To verify this hypothesis numerically we calculated the values of I' for each particle at the moment it crossed the equatorial plane, that is, our $z = 0$ detector. For these calculations we used the analytical expression (6) relating the value of I' with the angles α_0 and β_0 for the moment when the particle crossed the equatorial plane. This enabled us to obtain the distribution function $f(I')$ all over the magnetotail equatorial plane. The results of this calculation are plotted in Figure 8, which shows $f(I')$ averaged over $\Delta x = 10 R_E$ bins. Accordingly, the top panel in Figure 3 represents the

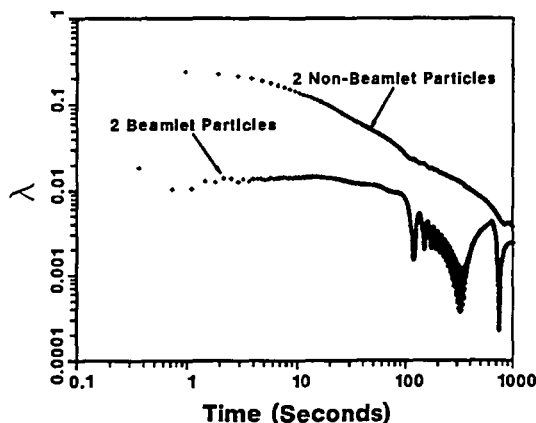


Figure 7. Plot of λ versus time (analog of Lyapunov exponent) for the two pairs of beamlet and nonbeamlet particles shown in Plate 4.

average for the interval $10 R_E < x < 20 R_E$, and the bottom panel represents the average over the interval $90 R_E < x < 100 R_E$. Of course, this averaging is too rough to reveal individual structures associated with resonances, but it gives us a very interesting picture of the overall evolution of $f(I')$ towards an isotropic angular distribution. The dotted line in each of these plots corresponds to $f(I')$ for an isotropic angular distribution calculated by Ashour-Abdalla *et al.* [1991]. In the distant tail (bottom panel), where mantle ions are first incident on the neutral sheet, there is an absence of ions with large I' values. Closer to Earth, between $x = 70$ and $90 R_E$, the distribution shifts towards larger I' values, as ions with small I' (beamlet particles) are ejected from the current sheet. Earthward, the beamlet particles return to the current sheet ($60 R_E < x < 70 R_E$), and the distribution slowly becomes isotropic (compare this with the dotted line showing $f(I')$ for a 1-keV Maxwellian distribution). This is consistent with observations reporting that the particle distributions in the middle and near-Earth parts of the magnetotail are nearly isotropic.

Figure 8 clearly illustrates the complicated structure of magnetotail plasma as basically containing two populations: (1) a bunched (collimated, "coherent") field-aligned part of the population associated with beamlets; energy gained by beamlet particles during their interactions with the current sheet is manifested in the form of the kinetic energy of their directed (roughly field-aligned) motion. This can be referred to as acceleration of beamlet particles, (2) As for other "scattered" parts of the population, the energy gained during the particles' interactions with the current sheet (as we argued above on an average it should have a value equal to approximately half of the beamlet energy) is manifested in a "randomized" form resembling thermal energy. Therefore in this case it is more accurate to call this process the energization of the population. As we will discuss in another paper the energy distribution created in the course of such acceleration should contain an essential non-Maxwellian tail, which might be described by a κ distribution with a particular value of κ depending on the topology of the magnetic field.

The "scattered" (chaotic) and regular (beamlet) populations coexist in the magnetotail until the regular (beamlet) population gradually converges to the scattered (chaotic) one as a result of the unavoidable scattering which occurs during each subsequent interaction with the current sheet.

The answer to the question of the extent to which deterministic chaos influences the formation of the ion distribution function in the magnetotail is two-fold: (1) these effects are very important for the scattered part of the magnetotail population and rather quickly randomize it; (2) for the beamlet population, which experiences far fewer scattered interactions, these effects become important only in the near-Earth tail and do not prevent the existence of very well defined structures in the vast regions of the distant and middle parts of the tail. Of course, both the strong chaotic scattering and almost regular (Speiser-type) acceleration are just two aspects of the same nonlinear process of ion interaction with a magnetic field reversal.

Plate 5 shows the near-Earth transition to the almost completely randomized system. The plate has four panels with distribution functions $f(v_x, z)$ taken at four neighboring x detectors $x = 30, 20, 12, 10$. In this plate the ion distribution is plotted in z - v_x space at different x locations. At $x = 30$ the magnetotail distributions have the "usual" form with a rather hot ($W \sim 6$ – 7 keV) central plasma sheet and a very well defined PSBL with streaming/counterstreaming accelerated ion beams having large energies

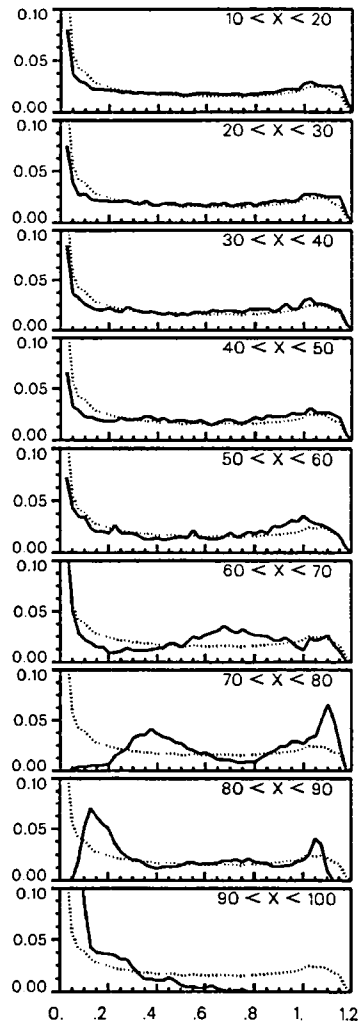


Figure 8. Plots of $f(I')$ versus I' for $10 R_E$ bins in x from $x = 10 R_E$ to $x = 100 R_E$. The solid line in each panel corresponds to results from our simulations, and the dotted line represents $f(I')$ for an idealized isotropic distribution.

(up to 16 keV in our model). In moving from $x = 30$ to $x = 10$ the PSBL streams gradually become narrower and lose energy, while the CPS becomes denser and hotter. These plots illustrate how the very large directed energy of PSBL flows is transformed to the quasi-thermal energy of CPS plasma. As our model does not assume the existence of specific dissipation mechanisms, this process may be referred to as a purely collisionless "geometrical" transformation of directed energy into the randomized energy of the CPS plasma.

The heating of the CPS occurs in the absence of any collisions or wave particle interactions which usually are assumed as absolutely necessary ingredients of such a transformation. We called this transformation geometrical because it occurs for rather simple geometrical reasons. By the time the near-Earth part of the tail is reached with its strong magnetic field, more and more PSBL (beamlet) particles get reflected and experience multiple interactions with the current sheet until all the particles get

scattered and all the beamlets are entangled and mixed into one hot quasi-isotropic CPS population. In convecting further towards Earth this distribution acquires a new anisotropy ($P_{\perp} > P_{\parallel}$) as a result of the predominance of betatron acceleration over Fermi acceleration [Cowley and Ashour-Abdalla, 1975; Ashour-Abdalla *et al.*, 1994].

This collisionless transformation of the directed kinetic energy of PSBL beams (or beamlets) into a quasi-isotropic CPS population resembles the process of chaotization of trajectories by multiple reflections from the walls in so-called mathematical billiards. This phenomenon definitely deserves much more theoretical attention, but here we address only its role in beamlet evolution, because it provides a sort of sink (CPS plasma) where eventually almost all beamlet particles bring their energies, get mixed, and lose their identities.

6. Summary and Discussion

In this paper we develop further the idea of spatial structuring of magnetotail plasmas which is intrinsically related to the nonlinear properties of the acceleration of solar wind protons during their interactions with the current sheet. We started with the example of ISEE measurements indicating the existence of beamlets (spatial structuring) in the near-Earth ($\sim 20 R_E$) plasma sheet boundary layer and continued with a numerical analysis of their interference and evolution in the magnetotail. Let us first summarize our findings.

1. The PSBL is formed of well-defined spatially separated beamlets, each characterized by strong Earthward or tailward flows. At the edges of the beamlets diamagnetic effects can produce significant dawn or duskward flows. The spatial distribution of the beamlets and their velocity dispersion are fully consistent with the separatrix theory of nonlinear acceleration and structuring.

2. The presence of beamlets also results in the significant structuring of the CPS. Although the tailward/Earthward velocities in the CPS are much lower than in the PSBL due to the geometry of the field density, inhomogeneities created by the beamlets can result in significant duskward/dawnward flows in this region.

3. We have shown that beamlets keep their identities until they have undergone up to a few interactions with the current sheet, and the interference of tailward- and Earthward-moving parts of various beamlets create a complicated mosaiclke spatial distribution of plasma bulk parameters almost throughout ($x > 65 R_E$) the magnetotail.

4. Magnetotail plasma is characterized by the coexistence of two well-defined populations: (1) an accelerated "ordered" population with small I' values having its energy mainly in the form of the kinetic energy of field-aligned motion and (2) a "scattered" energized population with large I' having its energy mainly in a quasi-thermal form and produced by the chaotic scattering of ions during their interaction with the current sheet. The relative contribution of these populations varies along and across the magnetotail. The distant CPS is formed mainly by the second population; nearer Earth, reflected beamlet particles from the first population also make an important contribution to the CPS population. The PSBL consists predominately of accelerated population (first population) ions.

5. In the near-Earth tail the accelerated and the energized populations finally intermix with each other and form a hot, almost isotropic plasma sheet. The kinetically directed energy of the majority of the beamlet particles (except a small precipitated

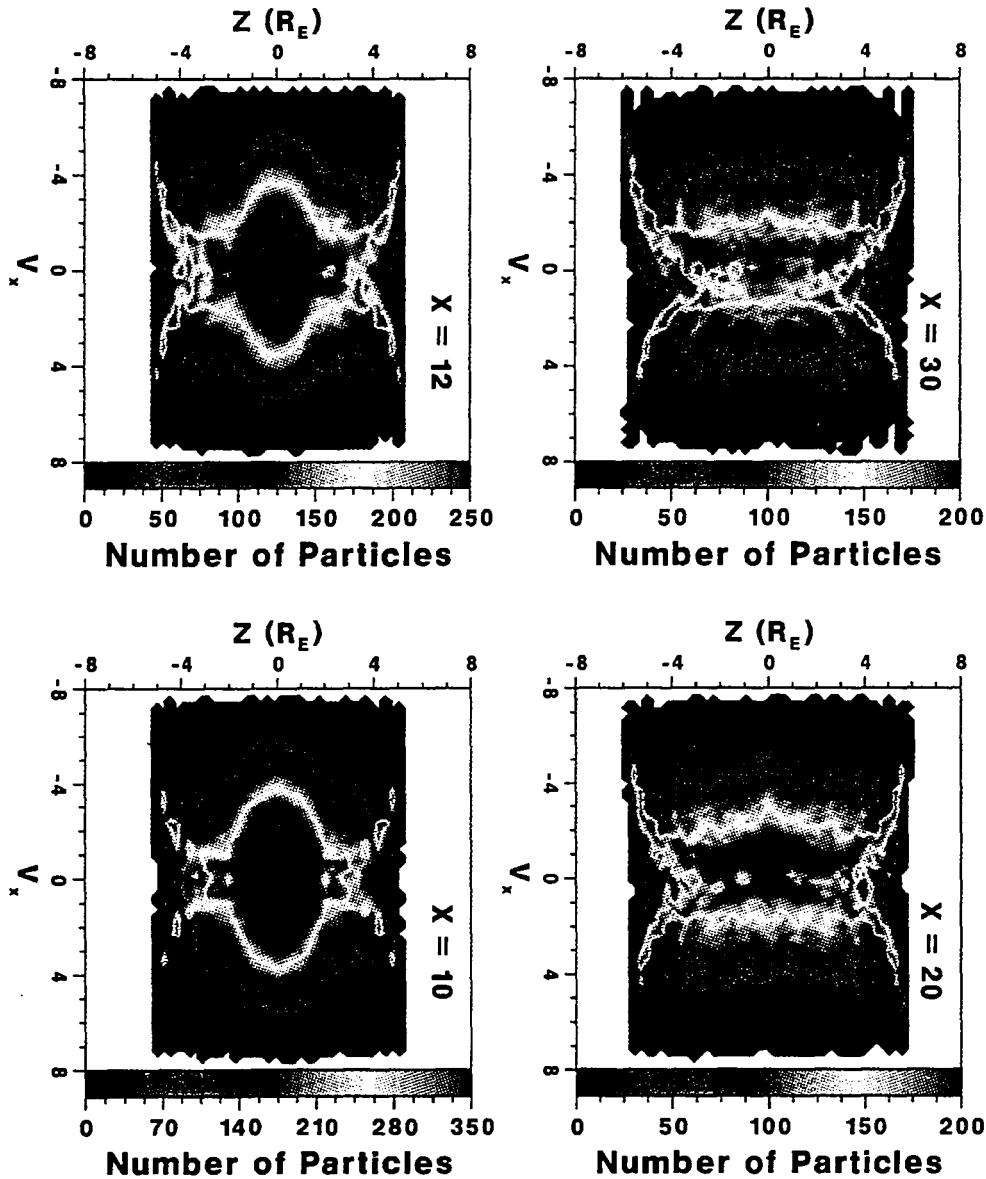


Plate 5. Ion distribution plotted in z - V_x space at different x locations. The color coding denotes particle flux, and V_x is shown normalized to $V_{th} = 240$ km/s. The plate illustrates the isotropization of plasma in the near-Earth CPS and the conversion of directed kinetic energy of PSBL beams into quasithermal energy.

fraction) is converted to the thermal energy of the CPS. The distribution function over I' evolves into the distribution characteristic for the isotropic one.

In all the results listed above the key element is the presence of spatial structuring found in our large-scale kinetic model. However, each model has its limitations, and one could argue that this principal effect will survive further generalizations of the model.

The important question, which will require more theoretical effort and which cannot be analyzed in the present modeling setup, is in what way do self-consistent wave particle interactions and particularly broadband electrostatic noise (BEN) contribute to the smearing of the beamlets. Results from previous studies

[Schriver and Ashour-Abdalla, 1991] indicate that the intensity of BEN is usually low enough so that it does not cause appreciable spatial smearing of the beamlets and may result in some widening of their initially very narrow velocity distribution.

Another concern might be related to the two-dimensionality of the model discussed above. Since the mechanisms responsible for the formation of structures are local, the generalization of our results to 3D should not alter the basic picture, even though the spatial distribution and velocity dispersion of three-dimensional structures might be quite different than those for two-dimensional space. This conjecture was tested in our new series of three-dimensional runs of the LSK model. The model itself and the main result drawn from it will be discussed in detail in another

X Bulk Velocity in the Noon-Midnight Meridian

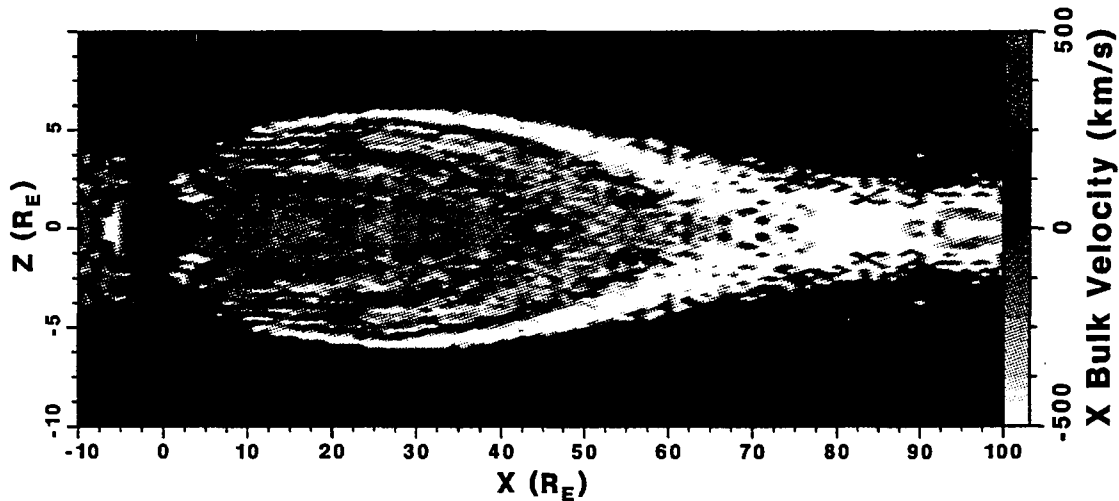


Plate 6. The x component of the bulk velocity calculated in the noon-midnight meridian for a 3D simulation using the Tsyanenko magnetic field model and an electric field derived from the *Heppner and Maynard* [1987] ionospheric potentials.

publication. Here we show only one plate (Plate 6) illustrating the pattern of the X component of the bulk velocity distribution in the noon-midnight meridional plane. The plate shows a marked qualitative similarity to those obtained from two-dimensional models, which confirms that the beamlets and their interference mosaic are as well reproduced by full three-dimensional modeling as by two-dimensional modeling.

The existence of the mosaic pattern of the bulk plasma parameters in the tail motivates very important consideration of the relationship between the MHD and the kinetic descriptions of the magnetotail plasma. One of the most striking results of LSK modeling of plasma distributions is how the plasma in the magnetotail can differ on certain spatial scales from the convecting fluid implied by the MHD approximation. As we have shown recently, we know from calculating moments of plasma distribution functions [Ashour-Abdalla *et al.*, 1994] after spatial averaging, that the LSK picture is basically consistent with the results of the MHD approach. The pattern of large-scale flows shown in Figure 2 also shows this agreement. However, a multitude of new physical effects emerges when we look at this distribution with a "magnifying glass" and retain the finer-scale spatial effects. As we have argued above, the plasma in the tail consists of a combination of a quasi-isotropic (scattered) population, which may be described by a fluid approximation and a separate system of interpenetrating interfering beams weakly interacting with each other. There are no mechanisms for the relaxation of such a structure on the timescale of their convection toward the Earth until, after numerous reflections in the inner central plasma sheet, they become naturally geometrically entangled and isotropized. By this process they collisionlessly convert their directed energy into quasithermal energy. MHD definitely fails to describe this process.

This situation in a way resembles that of collisionless shocks. On an average (at very large scales) they should always satisfy

the MHD Rankine-Hugoniot conditions, but in collisionless plasmas they have very complicated internal structures which provide the real physical mechanisms of plasma relaxation and conversion of directed energy into heat.

A similar consideration might be relevant to essentially non-Maxwellian and nonisotropic magnetotail plasmas, which can be viewed as a convecting fluid only in a global spatial scale, but at intermediate spatial scales these plasmas should already have a rather sophisticated internal structure.

As we have shown above, results from the large-scale averaging of the bulk flow pattern in the CPS shown in Figure 2 conforms well with the $\mathbf{E} \times \mathbf{B}$ convection motion of the plasma and therefore agrees with the experimental data similarly averaged over large scales [e.g., Angelopoulos *et al.*, 1993]. However, an analysis of the same pattern for smaller (intermediate in our notation) scales demonstrates a completely different picture.

Figure 9 shows the scatter plots of the bulk velocity obtained from our modeling results at $x = 30 R_E$ in the $|\Delta z| < 1.5 R_E$ interval around the equatorial plane. To produce these plots we averaged the value of V_x inside the small pixels (5800×1600 km) from which our mosaic pattern is produced. The values of V_x are similar in few neighboring pixels (which altogether form the patchy mosaic with the given value of v_x). As we can see the scatter is large, of the order of the average value of V_x . Angelopoulos *et al.* [1993] obtained similar results in the quiet CPS but interpreted them as oscillations of the electric field.

We, however, propose in this paper a different physical mechanism for explaining this scatter or variability of V . Each velocity vector shown in our plot corresponds to the actual bulk velocity measured in the particular spatial location coinciding with our pixel, and that should be exactly the value of bulk velocity that will be "instantly" measured at this location by spacecraft.

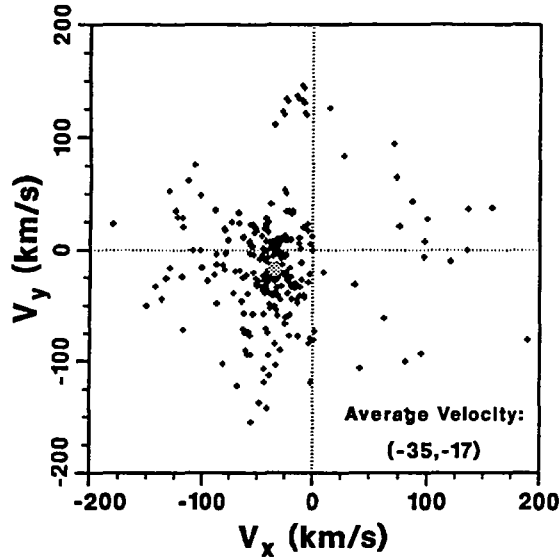


Figure 9. Scatter plot of V_x versus V_y for the region $x = 28.5$ to $31.5 R_E$, $y = 0.5$ to $-2.5 R_E$, and $|z| < 1.5 R_E$. The large gray circle represents the average bulk flows in the region.

This scatter therefore reflects the real complexity of the magnetotail plasma and the existence of structures in it, that is, principally the non-MHD behavior. (Recall that in our model, flow is stationary ($\partial B/\partial t = 0$) and $E = E_y = \text{const.}$) Differences between the MHD and large-scale kinetic descriptions become especially dramatic in the very distant tail where due to the weakness of $B_n(x)$, the regions of non-MHD behavior could become huge: in the tens of R_E . We have discussed a very pronounced example of it at the end of section 4 in relation with the $20-R_E$ difference in reversals of v_x and $B_z(x)$. This is a purely non-MHD effect related to rather "exotic" properties of ion trajectories in this region (very large local Larmor radius). The same effect on smaller (but still relatively large scales) occurs at other parts of the tail.

As we demonstrated here, the required variability of the plasma sheet on intermediate scales can be maintained by a constant and homogeneous electric field, and only in situ direct measurements of E are capable of giving its local value; that is, it cannot be directly derived from MHD equations at small and intermediate scales. So although on large spatial scales the magnetosphere as well as its numerical model behave like an MHD object, it may be meaningless to use MHD equations for making direct comparisons with local in situ measurements (unless they are averaged over large spatial regions).

Thus the existence of structuring brings new physical mechanisms to intermediate (below MHD) scales. The local picture now appears to be quite different from the large-scale one. Each process has its intrinsic scales and in moving to finer and finer resolution we should see quite new effects, which should not be surprising. One could even speculate that the hierarchy of scales is not exhausted at the large-scale kinetic mosaic pattern. By developing more sophisticated models we might see even smaller scale effects. The construction of this hierarchy (with our mosaic being just one of its steps) is truly a challenging goal, but one which is beyond the scope of this particular paper.

Acknowledgments. The authors wish to thank R. J. Walker, D. Schriver, J. Berchem, and L. A. Frank for their useful comments. The authors would also like to thank E. Luu for help with computing. The work at UCLA was supported by NASA ISTP grant NAG5-1100 and University of Iowa subcontract V26073. Work at CESR was supported by CNRS grant GdR Plasma and CNES under grant 8002A. One of the authors (Lev Zelenyi) is grateful to the International Science Foundation (Soros Fund) and the Russian Foundation for Fundamental Science grant 94-02-04-663 for partial support during this study. Computing was performed at the Office of Academic Computing at UCLA and at the San Diego Supercomputer Center.

The Editor thanks G. R. Burkhart and another referee for their assistance in evaluating this paper.

References

- Anderson, K. A., et al., An experiment to study energetic particle fluxes in and beyond the Earth's outer magnetosphere, *IEEE Trans. Geosci.*, **16**, 213, 1978.
- Andrews, M. K., P. W. Daly, and E. Keppler, Ion jetting at the plasma sheet boundary layer: Simultaneous observations of incident and reflected particles, *Geophys. Res. Lett.*, **8**, 987, 1981.
- Angelopoulos, V., W. Baumjohann, C. F. Kennel, F. V. Coroniti, M. G. Kivelson, R. Pellat, R. J. Walker, H. Lühr, and G. Paschmann, Bursty flows in the inner central plasma sheet, *J. Geophys. Res.*, **97**, 4027, 1992.
- Angelopoulos, V., et al., Characteristics of ion flow in quiet state of the inner plasma sheet, *Geophys. Res. Lett.*, **20**, 1711, 1993.
- Ashour-Abdalla, M., J. Büchner, and L. M. Zelenyi, The quasi-adiabatic distribution in the central plasma sheet and its boundary layer, *J. Geophys. Res.*, **96**, 1601, 1991a.
- Ashour-Abdalla, M., J. Berchem, J. Büchner, and L. M. Zelenyi, Large and small scale structures in the plasma sheet. A signature of chaotic motion and resonance effects, *Geophys. Res. Lett.*, **18**, 1603, 1991b.
- Ashour-Abdalla, M., L. M. Zelenyi, J. M. Bosqued, V. Peromian, Z. Wang, D. Schriver, and R. L. Richard, The formation of the wall region: Consequences in the near Earth magnetotail, *Geophys. Res. Lett.*, **19**, 1739, 1992.
- Ashour-Abdalla, M., J. P. Berchem, J. Büchner, and L. M. Zelenyi, Shaping of the magnetotail from the mantle: Global and local structuring, *J. Geophys. Res.*, **98**, 5651, 1993.
- Ashour-Abdalla, M., L. M. Zelenyi, V. Peromian, and R. L. Richard, Consequences of magnetotail ion dynamics, *J. Geophys. Res.*, **99**, 14,891, 1994.
- Baumjohann, W., G. Paschmann, and C. A. Cattell, Average plasma properties in the central plasma sheet, *J. Geophys. Res.*, **94**, 6597, 1989.
- Baumjohann, W., G. Paschmann, and H. Lühr, Characteristics of high-speed ion flows in the plasma sheet, *J. Geophys. Res.*, **95**, 3801, 1990.
- Belova, E. V., L. M. Zelenyi, O. L. Vaisberg, and R. L. Himenes, Plasma clouds in magnetotail lobes, *Cosmic Res., Engl. Transl.*, **25**, 464, 1987.
- Bosqued, J. M., AUREOL-3 results on ion precipitation, *Phys. Scr.*, **18**, 158, 1987.
- Bosqued, J. M., M. Ashour-Abdalla, M. El Alaoui, V. Peromian, L. M. Zelenyi, and C. P. Escoubet, Dispersed ion structures at the poleward edge of the auroral oval: Low-altitude observations and numerical modeling, *J. Geophys. Res.*, **98**, 19,181, 1993.
- Büchner, J., Correlation modulated chaotic scattering in the Earth's magnetotail, *Geophys. Res. Lett.*, **18**, 1595, 1991.
- Büchner, J., and L. M. Zelenyi, Deterministic chaos in the dynamics of charged particles near a magnetic field reversal, *Phys. Lett. A*, **118**(8), 395, 1986.
- Büchner, J., and L. M. Zelenyi, Regular and chaotic charged particle motion in magnetotail-like field reversals, 1, Basic theory of trapped motion, *J. Geophys. Res.*, **94**, 11,821, 1989.
- Burkhart, G. R., and J. Chen, Differential memory in the Earth's magnetotail, *J. Geophys. Res.*, **96**, 14,033, 1991.
- Burkhart, G. R., J. F. Drake, and J. Chen, Structure of the dissipation region during magnetic reconnection in collisionless plasma, *J. Geophys. Res.*, **96**, 11,539, 1991.
- Chen, J., and P. J. Palmadesso, Chaos and nonlinear dynamics of single-particle orbits in a magnetotail-like magnetic field, *J. Geophys. Res.*, **91**, 1499, 1986.
- Cowley, S. W. H., and M. Ashour-Abdalla, Adiabatic plasma convection in a dipole field: Variation of plasma bulk parameters with L , *Planet. Space Sci.*, **23**, 1527, 1975.

- DeCoster, R. J., and L. A. Frank, Observations pertaining to the dynamics of the plasma sheet, *J. Geophys. Res.*, **84**, 5099, 1979.
- Eastman, T. E., L. A. Frank, W. K. Paterson, and W. Lennartsson, The plasma sheet boundary layer, *J. Geophys. Res.*, **89**, 1553, 1984.
- Eastman, T. E., L. A. Frank, and C. Y. Huang, The boundary layers as the primary transport regions of the Earth's magnetotail, *J. Geophys. Res.*, **90**, 9541, 1985.
- Forbes, T. G., E. W. Hones Jr., S. J. Bame, J. R. Asbridge, G. Paschmann, N. Sckopke, and C. T. Russell, Evidence for the tailward retreat of a magnetic neutral line in the magnetotail during substorm recovery, *Geophys. Res. Lett.*, **8**, 261, 1981a.
- Forbes, T. G., E. W. Hones Jr., S. J. Bame, J. R. Asbridge, G. Paschmann, N. Sckopke, and C. T. Russell, Substorm related plasma sheet motions as determined from differential timing of plasma changes at the ISEE satellites, *J. Geophys. Res.*, **86**, 3459, 1981b.
- Green, J. L., and J. L. Horwitz, Destiny of Earthward streaming plasma in the plasma sheet boundary layer, *Geophys. Res. Lett.*, **13**, 76, 1986.
- Heppner, J. P., and N. C. Maynard, Empirical high-latitude electric field models, *J. Geophys. Res.*, **92**, 4467, 1987.
- Hones, E. W., Jr., and K. Schindler, Magnetotail plasma flow during substorms: A survey with IMP 6 and IMP 8 satellites, *J. Geophys. Res.*, **84**, 7155, 1979.
- Hones, E. W., Jr., J. R. Asbridge, S. J. Bame, M. D. Montgomery, S. Singer, and S. I. Akasofu, Measurements of magnetotail plasma flow mode with Vela 4B, *J. Geophys. Res.*, **77**, 5503, 1972.
- Huang, C. Y., and L. A. Frank, A statistical study of the central plasma sheet: Implications for substorm models, *Geophys. Res. Lett.*, **13**, 652, 1986.
- Huang, C. Y., L. A. Frank, and T. E. Eastman, Observations of plasma distributions during the coordinated data analysis workshop substorm of March 31 to April 1, 1979, *J. Geophys. Res.*, **92**, 2377, 1987.
- Liu, W. W., and T. W. Hill, Velocity filter effect and dynamics of distant magnetotail, *Planet. Space Sci.*, **24**(2), 197, 1986.
- Lui, A. T. Y., E. W. Hones Jr., F. Yasuhara, S. I. Akasofu, and S. J. Bame, Magnetotail plasma flow during plasma sheet expansions: VELA 5 and IMP 6 observations, *J. Geophys. Res.*, **82**, 1235, 1977.
- Lyons, L. R., and T. W. Speiser, Evidence for current sheet acceleration in the geomagnetic tail, *J. Geophys. Res.*, **87**, 2276, 1982.
- Martin, R. F., Chaotic particle dynamics near a two-dimensional neutral point, with application to the Earth's magnetotail, *J. Geophys. Res.*, **91**, 11,985, 1986.
- Möbius, E., F. M. Ipavich, M. Scholer, G. Gloekler, P. Hovestadt, and B. Klecker, Observations of a nonthermal ion layer at the plasma sheet boundary during substorm recovery, *J. Geophys. Res.*, **85**, 5143, 1980.
- Moses, R. W., J. M. Finn, and K. M. Ling, Plasma heating by collisionless magnetic reconnection: Analysis and computation, *J. Geophys. Res.*, **98**, 4013, 1993.
- Ohtani, S., R. C. Elphic, C. T. Russell, and S. Kokubun, ISEE-1 and -2 observations of an isolated diamagnetic event: An Earthward-moving bulge or a tail-aligned flux rope, *Geophys. Res. Lett.*, **19**, 1743, 1992.
- Parks, G. K., C. S. Lin, K. A. Anderson, R. P. Lin, and H. Reme, ISEE 1/2 observations of outer plasma sheet boundary, *J. Geophys. Res.*, **84**, 6471, 1979.
- Parks, G. K., et al., Particle and field characteristics of the high-latitude plasma sheet boundary layer, *J. Geophys. Res.*, **89**, 8885, 1984.
- Schriver, D., and M. Ashour-Abdalla, Cold plasma heating in the plasma sheet boundary layer: Theory and simulations, *J. Geophys. Res.*, **95**, 3987, 1990.
- Schriver, D., and M. Ashour-Abdalla, Consequences of wave-particle interactions on chaotic acceleration, *Geophys. Res. Lett.*, **18**, 1607, 1991.
- Sonnerup, B. U. O., Adiabatic particle orbits in a magnetic null sheet, *J. Geophys. Res.*, **76**, 8211, 1971.
- Speiser, T. W., Particle trajectories in model current sheets, 1, Analytical solutions, *J. Geophys. Res.*, **70**, 4219, 1965.
- Takahashi, K., and E. W. Hones Jr., ISEE 1 and 2 observations of ion distributions at the plasma sheet-tail lobe boundary, *J. Geophys. Res.*, **93**, 8558, 1988.
- Tsyganenko, N. A., A magnetospheric magnetic field model with a warped tail current sheet, *Planet. Space Sci.*, **37**, 5, 1989.
- Williams, D. J., Energetic ion beams at the edge of the plasma sheet: ISEE 1 observations plus a simple explanatory model, *J. Geophys. Res.*, **86**, 5501, 1981.
- Zelenyi, L. M., R. A. Kovrazhkin, and J. M. Bosqued, Velocity-dispersed ion beams in the nightside auroral zone: AUREOL-3 observations, *J. Geophys. Res.*, **95**, 12,119, 1990.

M. Ashour-Abdalla and R. L. Richard, Institute of Geophysics and Planetary Physics, University of California, 405 Hilgard Avenue, Los Angeles, CA 90024-1567. (e-mail: mabdalla@igpp.ucla.edu; richard@igpp.ucla.edu)

J. M. Bosqued, Centre d'Etude Spatiale des Rayonnements, 9, Avenue du Colonel Roche, BP 4346, 31029 Toulouse Cedex, France. (e-mail: CNESTA::BOSQUED)

V. Perroomian, Space and Environment Technology Center, The Aerospace Corporation, P. O. Box 92957, Los Angeles, CA 90009 (e-mail: DIRAC2::PERROOMIAN)

L. M. Zelenyi, Space Research Institute, Academy of Sciences of Russia, 84/32 Profsoyuznaia, 117810 Moscow, Russia (e-mail: lzelenyi@esoc1.bitnet)

(Received September 8, 1994; revised March 3, 1995; accepted March 16, 1995.)

End of Document